REPORT DOCUMENTATION PAGE

AFRL-SR-BL-TR-99-

0198

Public reporting burden for this collection of information is estimated to average 1 hour per response, includ
gathering and maintaining the data needed, and completing and reviewing the collection of information. Sen
collection of information, including suggestions for reducing this burden, to Washington Headquarters Servic
Davis Highway, Suite 1204, Arlington, VA 22202-4302, and to the Office of Management and Budget, Paperwork

sources,
ct of this
Jefferson

1. AGENCY USE ONLY *(Leave Blank)*	2. REPORT DATE 01/29/99	3. REPORT TYPE AND DATES COVERED Final Technical Report; 04/01/97 - 09/30/98

4. TITLE AND SUBTITLE A Collaborative High Altitude Flow Facility (CHAFF): University Facility for Studies of High Altitude Propulsion Plumes, Liquids and Gas Releases, and Interactions ~~with their Environments~~	5. FUNDING NUMBERS F49620-97-1-0208 G 3484/US 61103D
6. AUTHORS E. Phillip Muntz, Fred Lutfy, Andrew Ketsdever, Steve Vargo	

7. PERFORMING ORGANIZATION NAME(S) AND ADDRESS(ES) Department of Aerospace Engineering University of Southern California 854 W. 36th Pl., RRB 101 Los Angeles, CA 90089-1191	8. PERFORMING ORGANIZATION REPORT NUMBER
9. SPONSORING / MONITORING AGENCY NAME(S) AND ADDRESS(ES) AFOSR/NA 110 Duncan Ave., Room B115 Bolling AFB, D.C. 20332-8050 Attn: Dr. Mitat Birkan	10. SPONSORING / MONITORING AGENCY REPORT NUMBER

11. SUPPLEMENTARY NOTES

12a. DISTRIBUTION / AVAILABILITY STATEMENT Approved for public release; distribution unlimited	12b. DISTRIBUTION CODE

13. ABSTRACT *(Maximum 200 words)*
See enclosure.

19990823 143

14. SUBJECT TERMS Ion propulsion, vacuum system, atmospheric simulation			15. NUMBER OF PAGES 37
			16. PRICE CODE

17. SECURITY CLASSIFICATION OF REPORT Unclassified	18. SECURITY CLASSIFICATION OF THIS PAGE Unclassified	19. SECURITY CLASSIFICATION OF ABSTRACT Unclassified	20. LIMITATION OF ABSTRACT UL

NSN 7540-01-280-5500

Standard Form 298 (Rev. 2-89)
Prescribed by ANSI Std. Z39-1
298-102

DTIC QUALITY INSPECTED 4

A Collaborative High Altitude Flow Facility (CHAFF): University Facility for Studies of High Altitude Propulsion Plumes, Liquids and Gas Releases, and Interactions

Fred M. Lutfy[†], Stephen E. Vargo[†], E. Phillip Muntz[††]
University of Southern California, Department of Aerospace Engineering, Los Angeles, CA

Andrew D. Ketsdever[‡]
Air Force Research Laboratory, Propulsion Directorate, Edwards AFB, CA

Interest in realistic simulation of the space environment as applied to the study of contamination and thruster plumes has led to the development of the CHAFF-4 facility. A multi-fin cryogenically cooled array (~20K) completely envelops the interior of the CHAFF-4 chamber, providing an available condensing surface area of 590 m². It is anticipated that the equivalent altitudes that can be simulated for various electric propulsion systems vary between 150-350 km (depending on type). The effective pumping speed is predicted to be about $9x10^6$ liters/sec. The facility is designed to accommodate thruster power levels up to 3500 W without the use of supplementary liquid helium, although infrastructure permitting its use is available. Provisions for the simulation of high-speed LEO flow environments have been incorporated in the design, and the corresponding pumping requirements are well within the capabilities of CHAFF-4. Developmental considerations and design issues are discussed based on the requirements of plume testing, in order to ensure the validity of phenomena that are observed in the facility. The construction of the CHAFF-4 facility required a period of about 12 months. It is now complete and preliminary leak checking has been accomplished. Performance testing and more sensitive leak checking in order to bring the facility to operational status will require about six months from the date of this report.

I. Introduction
Background
In early 1995 discussions between E.P. Muntz at the University of Southern California and D.P. Weaver and A. Ketsdever of the Air Force Research Laboratory (then the Phillips Laboratory) identified the need for a high altitude plume and thruster research and development facility. One motivation was the present lack of ground-based facilities that could be used to investigate the many thruster interaction phenomena associated with the LEO high speed, rarefied flow environment. A second objective was to provide a facility that would be able truly to simulate the low pressures experienced by thrusters in space. A matter of significance, particularly for electric thrusters such as the Hall effect devices that operate based on a discharge directly exposed to the space environment. The same objectives are also of vital importance for meaningful contamination studies.

Apart from technical features, the changing research environment for university, industry and government laboratories suggested that any major, unique facility of the type being formulated should be available to a broad community of users. Taking advantage of the relatively reasonable operating costs of a university based facility, the Collaborative High Altitude Flow Facility (CHAFF) was conceived as a place where synergistic government, university and industry research and preliminary development activities could be nurtured.

The CHAFF is actually a complex of four high-altitude flow devices (Fig.1) that are identified in historical order. CHAFF-1 is a cryogenically pumped small plume facility. CHAFF-2 is for the study of high-altitude liquid vaporization phenomena. CHAFF-3 is a microthruster test chamber. CHAFF-4 is the new contamination, thruster and plume diagnostics LEO flow simulator. The first three are already available at USC. This paper documents the design considerations and the unique capabilities of the new

---

[†] Research Assistant, Student Member
[††] A.B. Freeman Professor, Fellow
[‡] Senior Research Engineer, Senior Member

CHAFF-4 facility. It has been made possible by the financial support of the Air Force Office of Scientific Research, the Army Research Office and the University of Southern California. Drs. Mitat Birkan (AFOSR), David Mann (ARO), Jay Levine (AFRL), Ron Spores (AFRL) and Dean Len Silverman (USC) have provided both spiritual and material support. Dr. Keith Goodfellow (JPL) has been very helpful answering questions concerning electric thruster testing.

The untimely death of David Weaver, who was the initial government advocate of CHAFF and as such important to its existence, has motivated the facility's operators to re-name it in recognition of his contribution. The purpose of the facility reflects David Weaver's abiding interests in high altitude plume research and collaborative, scientific endeavors.

A. Overview of CHAFF-4

The complex interactions that thrusters encounter in space as well as the thruster's impact on satellite systems have brought about the need to test these devices in specially designed vacuum facilities. It is important to note that there are few, if any, present-day vacuum facilities that were built with an infrastructure specifically tailored to address the concerns of contamination and plume diagnostic science. A notable historical exception was JPL's Molsink installation [Stephens, 1966]. However, none of the current or past facilities provide a simulated LEO high-speed flow environment. More typical are vacuum vessels that maintain reasonable background pressures for the operation of various electric thrusters. The latter help determine minimum lifetime expectancy of thrusters as well as measure realistic performance parameters [McLean & Lesky, 1997 and Simpson & Wallace, 1997]. Such facilities provide effective test platforms for thrusters and are designed to determine operational constraints and parameters; however, they are not necessarily appropriate for detailed plume and contamination studies due to the relatively high background concentrations of propellant atoms/molecules. Unlike thruster lifetime test chambers, CHAFF-4 was designed from its inception as a state-of-the-art contamination and plume diagnostics facility, including the presence of a high-speed external flow environment. CHAFF-4 will enable operators to measure intrinsic contamination footprints for a wide variety of electric as well as modest chemical thrusters (up to 5 g/sec flow rate). In addition, detailed and accurate near plume characterizations will be possible for the same variety of thrusters. Achieving the design conditions for CHAFF-4 is possible since the flux of reflected and sputtered material back scattering into the volume(s) of interest is drastically reduced by a cryogenic array condensation pumping system (Sec. V). The array condenses thruster efflux by enhancing the probability of multiple interactions with cold surfaces (77 and 20 K) before propellant species can scatter back into the interior of the chamber.

The cryogenic array's capture mechanism is based mostly on geometric considerations and takes advantage of the predominantly diffuse reflections that ion and neutral species experience. The basic geometric concept is illustrated in Figs. 2-4a,b, where it is illustrated how the solid angle available for reflected/sputtered material to backscatter into the chamber's interior is minimized. It is critically important for reliable contamination and plume diagnostic surveys that potential interference from propellant species backscattered from the chamber walls be kept to a minimum. Hence, the reflected/sputtered species are forced to interact in a manner that greatly enhances the probability of encountering cold surfaces and condensing (first 77 K then 20 K) before having an opportunity to escape back into the flow volume of interest.

The low background concentration of propellant fragments and the external high-speed flow capability make CHAFF-4 a unique facility. It is clear that one such facility is worth having. It will not be clear until thruster research results from CHAFF-4 are available whether or not there is a need for more than one such facility. It is for this reason that the original CHAFF concept was to make CHAFF-4 available to the community of government, university and industry investigators.

B. Thruster and Plume Studies

The design of CHAFF-4 is derived from a few basic criteria that are outlined in this section. A convenient framework for the discussion are the principles of the rarefaction of exhaust plume interaction with

background gases formulated by Muntz et al [1970]. Although framed in terms of conventional nozzle expansions, for present purposes the Muntz et al concepts apply equally well to ion thrusters. The thruster exhaust has two characteristic lengths, the mean free path λ_j of the exhaust gases in the background gas and the distance from the thruster, r_p, that is essentially free from the penetration of background gas into the exhaust gas plume. These characteristic lengths are most conveniently defined along the centerline of the exhaust plume. Exhaust plumes universally appear to be radial expansions from a source near the thruster exit (providing the observation is made at greater than say 10 diameters from the exit). For nozzle expansion the radial flow is generally at high Mach number. The high-speed ions from an electric thruster have a much greater Mach number than typical nozzle expansions. Thus, in both cases the flow away from the thruster is radial and it can for present purposes be considered to come from a single pseudo source. The characteristic plume dimensions λ_j and r_p are measured from the source and have the form

$$r_p = K_1 \frac{T_h}{V_{ex}^2} \qquad (1)$$

$$\lambda_j = \frac{1}{\sqrt{2}\Omega_{jB} n_A} \qquad (2)$$

where for SI units K_1 is a constant of order 10^7. Also, n_A is the atmospheric or background number density and Ω_{jB} is the momentum transfer collision cross-section between the exhaust gas species and the atmosphere or background species. The term T_h is the thrust in Newtons and V_{EX} is the propellant's exhaust speed. Generally $\lambda_j > \lambda_A$ primarily because $\Omega_{jB} < \Omega_A$ where λ_A and Ω_A refer to the atmosphere's mean free path and its average collision cross-section respectively.

A plume Knudsen number can characterize the rarefied interaction between exhaust gases and the atmosphere and is defined by; $Kn_p = \lambda_j/r_p$. If $Kn_p \gg 1$ the interactions can be considered to be two separable molecular scattering events [Muntz et al, 1970]. One is the effective stopping of the exhaust gases relative to the atmosphere in a distance λ_j and the other is the diffusive penetration of the atmospheric gases into the plume gases to a distance r_p.

It is instructive to cast the description of exhaust plume interactions outlined above into the framework of ground based thruster and plume investigations. Consider the atmospheric mean free path λ_A, by 150 km it is equivalent to the dimensions of any reasonable ground based facility. Since $\lambda_j \geq \lambda_A$ for practically all circumstances of any significance it is clear that full scale thruster investigations relating to complete plume-background interactions are not possible. However, providing $r_p \ll \lambda_j$ as is the case for small nozzle thrusters or for electric thrusters, significant studies can be made of the near plume region (close to the thruster in analogy to the near wake region of re-entry vehicles). This is of course assuming that the thruster is not creating its own background gas in the facility. Thus, an initial requirement is that the facility provides an inner envelope that efficiently suppresses the reflection of thruster exhaust gases so that the large majority of background gas in the facility can be injected separately and be characteristic of the upper atmosphere, not products of the thruster exhaust gases. To accomplish this the entire inner surface of the facility must be a pumping surface. To the extent that thruster exhausts are more or less collimated the pumping surface might be reduced to a hemisphere or somewhat less if no atmospheric simulation or contamination studies are anticipated. Since both of the latter areas are central to CHAFF-4, it is obvious that having the entire inner surface as a pumping surface is required.

It is perhaps worthwhile to point out that for studying the basic operation of nozzle thrusters the penetration of background gas into the plume is in all cases far downstream of the thruster in terms of exit diameter (D_0). That is, $r_p \gg D_0$ because of the necessity for maintaining continuum flow conditions in the nozzle expansion. As a consequence the background pressure and composition for studying nozzle thruster operating characteristics is not particularly critical.

3

For ion electric thrusters there is an entirely different situation. Note from eq (1) that $r_p \sim 1/I_{sp}^2$. For a fixed thrust, it is not surprising that the background is basically free to penetrate to the thruster exit in these devices. Thus, investigation of ion electric thruster operations in a facility is potentially much more sensitive to facility induced background conditions. In fact such effects may be very subtle since the background species (say Xe) generated by the thruster exhaust in the facility is the same as the propellant, consequently the effects of the background may be hard to discern. The approach adopted for CHAFF-4 was to design an extensive cryogenic finned array system that could effectively trap condensable species with little backscatter, basically acting as a molecular black-hole. The design is presented in Sec.V., along with estimates of its success.

C. Upper Atmospheric Flow Simulation

The injection of background or atmospheric species into CHAFF-4 cannot be done efficiently by simply leaking a gas into the facility since it will be pumped at great speed by the black-hole molecular pump discussed earlier. The injection can be accomplished by using a variant (large) of a continuum source molecular beam [Lebéheu & Campargue, 1997]. The continuum source creates a hypersonic beam of molecules from a differentially pumped, skimmed free jet or nozzle expansion. The expansion can be generated by a variety of techniques that have been used for the generation of fast atomic oxygen (AO) and ion beams, as reviewed in Sec.IV.

II High Altitude Background Density Considerations

Background Number Density

For the study of space thrusters in a ground facility there are three basic propellant populations that need to be addressed;

- energetic ions (100 to 3000 eV) from Hall effect and conventional ion thrusters along with a smaller number of very fast neutrals resulting from charge exchange,

- cold neutrals from the unionized component of ion thrusters (up to 50% of mass flow) as well as from cold or resistojet nozzle thrusters,

- fast neutrals (~1 eV) from chemical or arc discharge nozzle thrusters.

The objective of the CHAFF-4 design effort was to achieve an extremely small background concentration of propellant gas. Consider the characteristics of a typical thruster test facility with an internal surface area that has some relatively modest fraction (f_p) occupied by pump inlets or pumping surface. The exhaust mass flow ($\dot{M}_{EX}$) of a test thruster is generally stopped and randomized by the facility's surfaces. The random motion of the scattered propellant molecules drives them into the pump inlets. This model can be used to calculate the background number density of propellant, $n_{B,pr}$, as :

$$n_{B,pr} = \dot{M}_{EX} \left(\frac{T_P}{T_B} \right)^{\frac{1}{2}} \left/ \left[\frac{m_{pr}}{4} \left(\frac{8kT_P}{\pi m_{pr}} \right)^{\frac{1}{2}} f_p A_s \right] \right. \qquad (3)$$

where m_{pr} and T_P are respectively the mass of the propellant molecule and the temperature of the propellant gas as it is driven to the pumping surface (for cryosorption pumps this is about 80 K). T_B is the background gas temperature and A_S is the chamber's surface area.

Consider a thruster operating on xenon with $\dot{M}_{EX} = 5\times10^{-6}$ kg/s exhausting into a chamber of surface area A_s. From eq (3)

$$n_{B,pr} = \frac{4.2 \times 10^{17}}{f_p A_s} \tag{4}$$

A typical f_p might be 0.05 . For example, the TRW electric thruster test chamber [McLean & Lesky, 1997] has a fractional nominal pump inlet area of about 0.08. However the effective pumping area appears to be around 0.5 to 0.84 times this area probably due to conductance losses in the pumps (obtained by comparing predicted volume flow over nominal inlet are at T = 80 K to observed pumping speeds as quoted in McLean & Lesky, [1997]). Using an f_p of 0.75 x .08 in eq (3) along with A_s = 41m² gives $n_{B,pr}$ = 1.7 x 10^{17} m⁻³. The Hughes facility [Hughes, 1998] has an A_s = 290m² and an effective f_p = 0.087 leading to an $n_{B,pr}$ = 1.7 x 10^{16} m⁻³. This can be compared to an estimate of the neutral gas density exiting the thruster (say 0.10 m diameter) assuming a 400 m/s flow speed and that the neutral flow is 50% of $\dot{M}_{EX}$, giving n_N = 1.7 x 10^{18} m⁻³ close to the thruster exit. About 0.3 m from the exit the neutral plume density would be equal to the propellant background density. The high-speed ion number density is much less. Using an ion specific impulse of 3000 s (corresponding to a total thruster $I_{sp} \approx$ 1500 s) gives n_N = 7.5 x 10^{16} m⁻³. In order to decrease the background pressure relative to the direct thruster flow field concentration eq (4) suggests increasing f_p and A_s.

Randolph et al [1993] suggest that for studies of stationary plasma thruster operations reliable results can be obtained for $n_B \leq$ 1.6 x 10^{18} m⁻³. For near plume investigations they suggest $n_B \leq$ 4 x 10^{17} m⁻³. For other types of thrusters different criteria will apply. Randolph et al are silent on whether or not their criteria may have a thruster size or mass flow dependency. Clearly a critical point, at least for plume studies, is reached when the background mean free path $\lambda_B \leq l_f$, where l_f is the largest internal dimension of the facility. This condition can be expressed as

$$n_B \leq \left(\sqrt{2}\,\Omega_B l_f\right)^{-1} \tag{5}$$

For xenon the collision cross-section Ω_B is about 1 x 10^{-19} m² at 300 K and $n_B \leq$ 7 x $10^{18}/l_f$. Again for the TRW facility [McLean & Lesky, 1997] with an l_f = 5 m, $n_B \leq$ 1.4 x 10^{18} m⁻³. Note that this is about one order of magnitude greater than the n_B to be expected for a 5 x 10^{-6} kg/s mass flow in this facility. Apart from λ_B questions, the resonant charge exchange mean free path of xenon ions with xenon neutrals is, for 200 eV ions, estimated by Randolph, et al [1997] as Ω_{CE} = 4.2 x 10^{-19} m². The charge exchange criteria analogous to eq (5) is

$$n_B \leq \left(\Omega_{CE} l_f\right)^{-1} \tag{6}$$

where l_f depends on one's purposes, but if it is left as the maximum facility dimension, the TRW chamber gives $n_B \leq$ 4.8 x 10^{17} m⁻³ which matches the Randolph et al criteria.

Next it is of interest to look at issues raised by energetic ion sputtering. In order to suppress sputtering high-density carbon (graphite), a low yield target material, is used to shield the areas of high ion fluence at the chamber boundaries (Sec. V.). The discussion presented by Randolph et al indicates that even for stainless steel the backscatter contamination can be made acceptably small by having several meters between the thruster and the plume's primary impact area.

For reasons such as; investigations of back flow contamination, the effects of high-speed ambient flows on contamination, near plume characteristics, and thruster performance with flowing atmospheric species as the predominant background gas, it is important to maintain a very low propellant background gas contamination relative to the ambient atmosphere. The task of simulating the atmospheric background gas for various altitudes is outlined in Table 1. Using the 5 x 10^{-6} kg/s thruster xenon mass flow as before,

$n_{B,pr}$ is presented for the TRW (moderate size) and Hughes (large) facilities as examples of state-of-the-art test chambers.

Table 1: Parameters of interest for state-of-the-art electric thruster test facilities.

h (km)	n_A (m^{-3})	$\dot{m}_A$ (kg/m²s)	$n_{B,pr}$ (m^{-3})		$\dot{M}_A$ (kg/s) For simulation (4m² flow area)
			Medium	Large	
150	1 x 10^{17}	2 x 10^{-5}	1.7 x 10^{17}	1.7 x 10^{16}	8 x 10^{-5}
200	1 x 10^{16}	2 x 10^{-6}	1.7 x 10^{17}	1.7 x 10^{16}	8 x 10^{-6}
300	1 x 10^{15}	2 x 10^{-7}	1.7 x 10^{17}	1.7 x 10^{16}	8 x 10^{-7}

Note in Table 1 that the $n_{B,pr}$ is equal to n_A at 200 km for the large state of the art facility. The large facility has an $n_{B,pr}$ that is 17 times n_a at 300 km. In order to simulate the ambient atmosphere at 200 and 300 km (both operational satellite altitudes) it would be necessary to increase the effective pumping speed by at least a factor of 10 and preferably by 10². This is not going to happen by simply increasing the already large number of pumps (30) used in the large facility.

The design of CHAFF-4 is an attempt to take a new approach to this problem. Consider the sketches in Figs. 2-3 that show schematics of the CHAFF-4 pumping system. A test thruster operates on the facility centerline producing radial flow that is everywhere nearly tangent to the radially arrayed fins. Both the high-speed ions and the much slower speed neutrals impact the carbon surfaces on the LN$_2$ shield, and the He coolant supply tubes and the fin edges. Ions embed themselves in the carbon ejecting a carbon atom with a probability of about 0.03 (Sec.V.). The neutrals partially accommodate to the carbon surface and for the most part stick to the walls of the finned helium-cooled array. Some escape without sticking to a fin and return to the interior of the facility as background gas. There is scattering from the finite thickness of the fins, which also returns to the interior as background gas. Since the mean free path is large these background gas particles travel to some other portion of the pumping surface and condense with high probability. It is only those molecules that have a direction close to the normal of the two carbon coated surfaces that appear near the thruster as $n_{B,pr}$. Assuming that the majority of the thruster mass flow strikes the end wall of the pumping system the backscatter that reaches the position of the thruster exit diameter is:

$$\left(\dot{N}_{BS}\right)_i = \left(\dot{N}_{EX}\right)_i \left(F_{BS,Th}\right)_i \tag{7}$$

where i designates either an ion or a neutral and the fraction of backscattered propellant molecules to the thruster, $F_{BS,Th}$, is calculated using the following expression:

$$\left(F_{BS,Th}\right)_i = X_i A_{EX} \frac{\cos\Gamma}{\pi} \left[\frac{w}{(w+t)R^2} + \frac{t}{(w+t)(R-H')^2} \right] \tag{8}$$

where w is the spacing between plates, H' is the distance between the fin edge and the LN$_2$ shield, t is the thickness, A_{EX} is the area of the thruster's exhaust, R is the distance from the LN$_2$ shield to the thruster, X_i is either the ion sputtering coefficient or the neutral reflection coefficient and Γ is the effective angle between the thruster (assumed to be a point source) and the target door. Diffuse reflection is assumed for both the neutrals and sputtered products (Sec.V.).

The backscattered molecules that escape the condensing surfaces form a background gas of sputtered material and reflected neutrals as the particles travel to the next encounter with the condensing surface where they have a high probability of sticking. Some fraction of this material reaches the position of the

thruster a distance R from the LN_2 shield. Assume $\overline{V}$ is the average speed of the material reaching the thruster, thus from eq (7):

$$\left(n_{BS}\right)_{Th,i} = \frac{\left(\dot{M}_{EX}\right)_i \left(F_{BS,Th}\right)_i}{m_i \overline{V}_i A_{EX}} \tag{9}$$

where m_i is the propellant molecule mass. Eq. 8 can be evaluated for the unique panel geometry of CHAFF-4. For the ions ($i \equiv I$) the backscattered material number density $\left(n_{BS}\right)_{Th,I}$ = 7 x 10^{13} to 7 x 10^{11} m^{-3} depending on $\overline{V}_i$ and assuming $X_i = 0.03$ and $\dot{M}_{EX}$ = 5 x 10^{-6} kg/s. For the neutrals ($i \equiv N$) (assuming $\dot{M}_{EX}$ = 5 x 10^{-6} kg/s) the $\left(n_{BS}\right)_{Th,N}$ = 4 x 10^{15} m^{-3}. Compared to the facilities listed in Table 1, these figures represent 1-2 orders of magnitude improvement.

From a slightly different perspective the fraction of backscattered propellant molecules integrated over all possible backscattering directions is:

$$\left(F_{B.S.}\right)_{C,i} = X\left[\frac{w^2}{2H(w+t)} + \frac{t}{(w+t)}\right] \tag{10}$$

In this case the equation defining backscattered number density has the same form as Eq. 9 and can be written as:

$$\left(n_{BS}\right)_{C,i} = \frac{\left(\dot{M}_{EX}\right)_i \left(F_{BS,Th}\right)_{c,i}}{m_i \overline{V}_{c,i} A_c} \tag{11}$$

The area A_c is the vacuum chamber cross sectional area inside of the cryosurfaces and $V_{c,i}$ is close to the mean speed of the backscattered particles.

The backscattered number densities in Eqs (9) and (11) can be used to provide an effective pumping speed $\left(\dot{V}_i\right)$ for the facility by writing $\left(n_{BS}\right)_{Th,i} \dot{V}_{Th,i} = \left(n_{BS}\right)_{c,i} \dot{V}_{C,i} = \left(\dot{M}_{Ex}/m\right)_i$. Using Eqs (11) and (9) the expressions for the pumping speed are:

$$\dot{V}_{C,i} = \frac{\overline{V}_{C,i} A_c}{F_{BS,C,i}}$$

$$\dot{V}_{Th,i} = \frac{\overline{V}_{Th,i} A_{Ex}}{F_{BS,Th,i}} \tag{12}$$

For the CHAFF-4 cryosurface system the pumping speeds $\dot{V}_{C,i}$ and $\dot{V}_{Th,i}$ are about (see Sec. V. k) the same and are around 9 x 10^6 l/sec for the Fig 4(a) configuration. For predominantly neutral species pumping the backflow configuration illustrated in Fig. 4(b) is appropriate, this configuration would result in a facility pumping speed greater than 10^8 l/sec. More discussions on these points are presented in Sec. V.

A traditional expression for the maximum possible pumping speed of a chamber such as CHAFF-4 is [Moore, et al, 1989]:

$$\dot{Vol} = 12.1 \frac{D^3}{L} \tag{13}$$

where D and L are the chamber's diameter and length respectively, expressed in cm, and $\dot{Vol}$ is the conductance in liters/s. Equation 13 is representative of molecules undergoing diffuse reflections off the walls of the facility in a free-molecular flow regime. For a chamber with CHAFF-4's dimensions, the value of conductance is 5×10^5 l/sec. It is important to note that Eq. 13 does not appropriately describe cryogenic systems such as the type used in the CHAFF-4 facility. For instance, assume that all molecules from a source within a vacuum facility condense on a cryogenic surface when it is first encountered. The effective pumping speed for such a system would essentially be limited only by the flow rate of the source (forgeting any heat load related surface temperature increase) and is independent of the classic concept of chamber conductance. Thus the actual CHAFF-4 pumping speed of around 9×10^6 l/sec is more than an order of magnitude greater than the conventional limit pumping speed determined from Eq (13).

III. Thruster Test facilities and their characteristics

A. Thruster Test Facilities

During thruster operation, typical performance test facilities can maintain background pressures of order 10^{-5} Torr, which is high in comparison to what a thruster would encounter in space, but is low enough to perform reasonable lifetime and performance testing. The utilization of these ground-based facilities allow researchers to evaluate thruster performance and investigate specific thruster characteristics. Many university, government and industry laboratories have developed and utilized these types of chambers for investigating various aspects of propulsion systems. For the purposes of comparison to CHAFF-4 three representative chambers have been selected and are outlined in Table 2.

B. Overview of electric propulsion thrusters as chamber design drivers

This section provides an overview of some electric propulsion devices that are of current space interest and their corresponding requirements as design drivers for the CHAFF-4. Electric propulsion devices can be categorized by the following three groups: electrothermal, electrostatic and electromagnetic. These electric thrusters include; arcjets, resistojets, ion engines, Hall-effect thrusters and pulsed-plasma thrusters (ppts). In addition, modest chemical and cold gas thrusters can also be incorporated.

Table 3 summarizes some of the characteristics of commonly used electric thrusters in space applications [Filliben, 1997 and Mueller, 1997]. The use of a specific thruster in an evaluation facility creates various thruster-chamber issues. Some of the more important interactions are outlined in Table 4 [Filliben, 1996].

The degree of plume ionization and corresponding energy are key design criteria because of the adverse effects that high-energy propellant species have on the interior of the chamber. High-energy ions can cause erosive sputtering of chamber materials and subsequently generate a non-trivial population of species that can alter plume structure and contamination signatures. The exhaust beam divergence angle dictates the areas of high-energy interactions with surfaces, and hence, the placement of surface protection schemes (graphite). The ability to attain high-vacuum levels during thruster operation is dependent on the thruster type and its corresponding mass flow rate. The design of the CHAFF-4 targets most electric propulsion systems and could handle modest chemical thrusters (~5g/sec mass flow rates) as well, although for economic reasons its condensing surfaces are not resistant to chemically aggressive propellant species.

IV. CHAFF-4 Atmospheric Flow Simulation Requirements

The interactions between spacecraft thruster plumes and the ambient environment have been of interest to many communities for the past several years. The CHAFF-4 provides an opportunity to simulate a variety of on-orbit phenomenon relating to thruster operation. Applications to material degradation, spacecraft contamination, gas-surface interactions and, in particular, atmospheric plume interactions

Table 2: CHAFF-4 and three representative thruster evaluation chambers.

Chamber Designation	Chamber Size: diameter, m x length, m	Pumping Scheme	Designed Thruster Type	Design Mission
CHAFF-4 Medium	3 x 6.1	590 m² cryogenic surface, 2 one meter diameter diffusion pumps	Electric, Chemical, Microprop.	Contamination, Plume Diagnostics, Research and Preliminary Development
Medium (Dettleff, 1997)	3.3 x 6.6	30 m² LHe cylindrical surface	Chemical	Performance and Plume Diagnostics
Large, (Hughes, 1998)	6.1 x 12.2	30 cryopumps of 48" size (35m²) (TM-1200)	electric (Xenon ion)	Lifetime and Performance
Medium (McLean, 1997)	2.1 x 5.2	3 cryopumps of 48" size (3.5m²) (TM-1200)	electric (Hall Effect)	Performance and Evaluation

Table 3: Typical electric thruster characteristics [Filliben, 1997 and Mueller, 1997].

Thruster type	Propellant	Formula	Mass flow (mg/s)	Power required (kW)	Efflux species
Resistojet	Hydrazine, Water	N_2H_4, H_2O	up to 83	0.1-10	N,O,H, N_2,O_2,H_2 NH_3, OH
Arcjet	Hydrazine, Ammonia	N_2H_4, NH_3	20-240	0.5-26	N,H,N_2,H_2,NH_3
Xenon ion	Xenon	Xe	0.5-5	0.5-20	Xe
Hall Effect	Xenon	Xe	5-40	0.5-20	Xe
Microprop.	varied	varied	<1	0.001- 0.010	varied

Table 4: Chamber design issues for electric thruster usage (taken, in part, from Filliben, 1996).

Thruster type	Plume Ionization downstream	Plume energy level	Exhaust beam divergence angle, °	Chamber Design Impact
Resistojet	negligible	low	>45	high mass flow cryogenic pumping
Arcjet	slight (~ 1%)	low-moderate	>45	High power, high mass flow cryogenic pumping
Xenon ion	high	high	15-40	ion induced sputtering
PPT	variable	variable	>45	Teflon condensate
Hall Effect	high	moderate-high	45	ion induced sputtering

(plume signatures) are all of interest. Of particular interest in low-Earth orbit (LEO) is the interaction of thruster plume species with atomic oxygen (AO) [Vaghjiani, 1996] and solar ultraviolet radiation (SUV). Ion electric thruster plume interactions with the ambient plasma environment have also been of interest recently [Wang & Brophy, 1995]. The injection of background or simulated atmospheric species in CHAFF-4 can not be done efficiently by simply leaking a gas into the facility since it will be pumped

very effectively by the cryogenic system. The injection into the facility must be accomplished by using a variant of a continuum source molecular beam. The continuum source creates a hypersonic beam of molecules from a differentially pumped, skimmed free jet, nozzle, or ion source expansion (Fig. 3). The expansion can be generated by a variety of techniques that have been used for the production of energetic AO and ion beams as discussed in the following sections.

A. The Simulation of Atmospheric AO

Atomic oxygen is the predominant species in LEO between 180 and 650 km altitude. AO primarily in the ground (^{3}P) state, results from the photodissociation of molecular oxygen by SUV radiation. With typical number densities of 10^9 cm^{-3}, the flux of AO to surfaces normal to the satellite ram direction is approximately 10^{15} cm^{-2}sec^{-1}. In the thermosphere (>80 km), AO is present at nearly thermal energies (~ 0.01 eV); however, the relative kinetic energy encountered during collisions with LEO spacecraft (traveling at 8 km/sec) is about 5 eV. Therefore, AO interactions with thruster plumes generally fall into three categories:

(1) AO interactions with low energy (<10 eV), retro-fire plume species
(2) AO interactions with high energy (>10 eV), retro-fire plume species
(3) AO interactions with plume species of any energy in the anti-ram direction

For low energy, retro-fire plume studies, the energy of the atmospheric species (in this case AO) must be faithfully reproduced for accurate analysis. In this case, the AO energy of 5 eV becomes a significant fraction of the overall relative velocity of the collisional system, which tends to drive the chemical kinetic mechanisms. Chemical and electrothermal thrusters generate low energy plume species. However, the neutral species of a typical ion thruster are also at low energy. AO sources that can produce energies approaching 5 eV with adequate flux levels are generally complex and expensive systems. [Caledonia et al, 1987 and Orient et al, 1990]

For high energy (ion thruster) retro-fire or anti-ram plume studies, the energy of the atmospheric species is either unimportant (compared to the incident plume energy) or can be accurately simulated using thermal AO. This greatly simplifies the AO production scheme since energetic AO is not required; however, accurate simulation of anticipated flux levels is still important for studies trying to identify appropriate chemical kinetic mechanisms. Relatively simple microwave discharge production of AO can be used which provides thermal energies at appropriate flux levels [Van Zyl and Gealy, 1986].

An ideal AO source for plume related studies would be a tuneable energy, tuneable flux source like those initially investigated by Banks [1996] and his group at NASA Lewis Research Center and Ketsdever et al., [1994, 1995]. Although the investigations into these systems were limited in scope, they showed the potential for tuneable energy atomic beams produced by energy selected, charge exchanged ions. With these systems, collisional energy dependent studies would be possible regardless of the thruster configuration or operating direction.

Note that the anticipated mass flows associated with the use of high-speed atmospheric simulations are well within the pumping capabilities of CHAFF-4 (Table 1).

B. The Simulation of Ambient Plasma Constituents

The simulation of the ambient plasma environment is accomplished using an ion source that operates on nearly any gas [Ketsdever, 1995]. The ions are produced using a microwave discharge and accelerated to the appropriate energy through electrostatic grids. Electrons can be added downstream of the ion acceleration to charge neutralize the plasma. The ion source is capable of energies ranging from 20 eV to 5 keV. Fluxes on the order of 10^{15} cm^{-2}sec^{-1} are possible for nitrogen, oxygen and hydrogen discharge gases. Since the source operates on molecular gases such as N_2, O_2, and H_2, the desired ion (either molecular or atomic) can be mass selected prior to introduction into the main facility.

V. CHAFF-4

A. Summary of Design Objectives for CHAFF-4

The following is both a summary and overview of the necessary operational parameters that need to be considered before a successful contamination and plume facility can be built. Such a facility should feature effective elimination of facility created species in the plume and backflow regions due to sputtering and reflection processes. It should be relatively straightforward to mount and provide power, cables, etc. to a specific thruster and associated optical diagnostics package. The facility must be relatively user friendly and cost effective. The CHAFF-4 design effort used the following specifications and constraints to satisfy the conditions outlined above:

- Minimize interference by reducing concentrations of sputtered/reflected products to a level <<1% of natural plume and backflow number densities by using a series of unique cryogenically cooled panels as well as careful material selection;

- Precise and accurate sting mounted thruster and associated optical diagnostics package;

- 3-axis non-intrusive optical imaging capability which can be adjusted during a test run;

- Incorporate multiple optical and other ports of various sizes for diagnostics studies; laser-induced fluorescence (LIF), electron-beam fluorescence (EBF), quartz crystal microbalances (QCM), etc.;

- Quick as possible turn-arounds;
- Provide for O-atom, plasma and SUV generators to simulate LEO environment.

B. Chamber Design

In comparison to other thruster evaluation chambers the CHAFF-4 is a moderate size facility (Table 2) (Fig. 5). Figs. 3 & 5 show an outline of the CHAFF-4 chamber. On the back door two 1 m diffusion pumps have been placed to remove incondensable gases from the facility (typically He and H_2). An adjustable thruster support, which is referred to as the sting, is placed in the center of the castered door. The sting allows longitudinal movements of mounted thrusters and also carries a stepper motor optical system (Sec.VI.). Optical access to the interior of the chamber is made with several large (25 cm), medium (10 cm) and small (7 cm) viewports. The number and location of these viewports have been selected to provide reasonable diagnostic flexibility. Two viewing stations were placed at one-third and two-third chamber-length locations to provide for diagnostic measurements of thruster plumes in the chamber. Each station has three orthogonally placed 10 cm optical ports on the chamber wall (i.e. left side, top, right side). In addition to the 10 cm ports, each station has four 7 cm ports that are placed between the orthogonal ports. Quartz and Pyrex glass windows are used in these locations depending on the optical needs. Various vacuum, temperature, high-power, liquid and cryogenic feed-throughs are also placed on the chamber. The associated data acquisition/monitoring systems are implemented using two dedicated computers that are housed in a control room next to CHAFF-4. System monitoring areas include panel temperatures, LHe/LN$_2$ levels, cryostat operation, chamber pressure and roughing pump status. Both computers are fitted with data acquisition boards and components consistent with National Instruments' LabView software. Power failures and other complications that compromise the safe and efficient operation of CHAFF-4 initiate automated shutdown procedures.

C. Pumping System for Incondensable Gases

Conventional pumps are necessary to remove incondensable gases such as hydrogen and helium that the cryogenic pumping scheme discussed in the following sections is unable to pump from the system. Hydrogen and helium are present in the facility from normal atmospheric partial pressures but they can also be introduced as propellants in resistojet or arcjet studies or as atmospheric species. For this reason, the CHAFF-4 facility is conventionally pumped by two Zyrianka 900 diffusion pumps of Russian

manufacture that are shown in Fig. 6. The general dimensions and operating characteristics of the Zyrianka 900 are given in Table 5. Diffusion pumps were chosen for conventional pumping of the facility due to the high pumping speeds achievable and low cost per pumped volume. The major disadvantage to using oil diffusion pumps is the potential for chamber contamination from backstreamed pumping fluid.

Turbomolecular pumps, although capable of comparable pumping speeds for molecular hydrogen and nitrogen, are extremely expensive when compared on a cost per pumping speed level. Oil cooled bearings on turbomolecular pumps can also be a source of oil contamination in the chamber although at relatively low levels as compared with diffusion pumps. Although cryosorption pumps are about half as expensive per pumping speed as turbomolecular pumps, they also have their limitations. Cryosorption pumps can not pump large flow rates of hydrogen and helium for extended periods of time without regenerative procedures.

The major feature of the Zyrianka 900 diffusion pump is the backstreaming rate of approximately 24 mg/hr over the inlet diameter. This is nearly an order of magnitude lower backstreaming rate than diffusion pumps of similar size manufactured elsewhere. The Institute of Thermophysics of the Russian Academy of Sciences has developed the Zyrianka series of pumps by optimizing the interactions of the oil vapor jets with the jet assembly and the pump condensing walls to minimize the backstreaming of the pumping fluid. [Rebrov, 1990 and Iliasova et al, 1993] As can be seen by point 9 in Fig.6, the oil vapor ring jet from the first stage is pointed toward the pump axis. The effect of this first stage jet configuration is to make the cooled outer casing an effective trap of the backstreaming oil vapor flow even at large expansion angles [Rebrov, 1986]. A small water-cooled trap

Table 5: Technical specifications of the Zyrianka 900 diffusion pump.

Inlet Diameter (mm)	932
Height (mm)	1360
Pumping Speed (l/sec)	Air 25000 Helium 42000
Normal Operating Range (Torr)	5 x 10-4 to 10-8
Pumping Fluid Backstreaming (mg/hr)	24

is located on top of the ring jet staging to further reduce any oil backstreamed into the facility. If oil contamination in the chamber becomes an issue, contingencies that call for cryo-baffling on the liquid nitrogen panels inside the facility are available. Note the backstreaming is not directly critical to facility operation because CHAFF-4 has no cryosorption pumps, which are extremely sensitive to oil vapors.

D. Description of cryogenic panel system
Cryogenic facilities have historically been constructed with the maximum pumping area that could be reasonably incorporated [Hughes, 1998]. Although available pumping area is also a concern for CHAFF-4, the critical issue for a plume facility is minimizing sputtered and/or reflected products from the walls. Therefore, CHAFF-4's cryogenic shield arrays were designed to achieve both optimum pumping capability by reducing the flux of backscattered molecules to the lowest possible levels.

CHAFF-4 has three aluminum cryogenic systems partitioned into four independent sections (LN$_2$, gaseous He and liquid He). Aluminum was chosen since it was roughly half the cost of copper. For the finned configuration of CHAFF-4 simple stainless steel construction was not adequate because of thermal conductivity limitations on cooling line spacing. First, liquid nitrogen panels (LN$_2$) thermally isolate the chamber's walls from its interior. The coverage of LN$_2$ shields is significant (i.e. >99% of actual chamber wall area - Fig. 3). There is a total of 72 m^2 of LN$_2$ shields. The majority of this area (51 m^2) has a polished aluminum surface (emissivity of 0.05), and the remaining 21 m^2 has a surface property corresponding to graphite (emissivity of 0.95). The associated heat load on the interior of the chamber due to the LN$_2$ shields is approximately 12 W, assuming surfaces at 80 and 25 K. Second, the cryostat

reduces the interior shield's temperature to between 20-35 K as shown in Fig. 7. The cryostat's heat load capacity (Fig. 7) is more than adequate for ion engines and Hall-effect thrusters. The propellant of choice for these systems is xenon, which is very effectively pumped below ~50 K (Fig.13) [Lide, 1993 and Garner et al, 1996]. However, in order to have the flexibility of testing the full range of thrusters (arcjets, resistojets and modest chemical types), a lower operating temperature is required for the inner shields. Consequently, there is an option to use liquid helium to reduce the interior's temperature (<10 K) to combat any complications that stem from elevated heat loading and/or pumping requirements (Fig. 2). The liquid nitrogen shield system requires about 1 hour to cool down properly while the remaining cool down time from 77 K to ~25 K using the cryostat takes 10-24 hours.

The shields are shown in various perspectives in Figs. 2-4. Using geometric considerations to minimize backscatter was paramount and Figs. 4a,b graphically displays the concept. By allowing most thruster atoms through to impact the liquid nitrogen panels, two important issues are addressed:

- First, the solid angle available to atoms sputtered and reflected to the interior of the chamber is greatly reduced. Consequently, a reflected/sputtered atom from the LN_2 shield has a high probability of interacting with another cold surface (25 K) before returning to the chamber's interior.

- Second, the liquid nitrogen panels effectively handle roughly 85% of the total heat load produced by thrusters, thereby allowing the cryostat's heat load capability to be used for pumping predominantly thermal atoms rather than wasting available power battling energetic species.

E. Cryogenic Pumping System
An integral component of CHAFF-4's unique pumping scheme is a closed-loop gaseous helium refrigeration system. This system, which is referred to as the cryostat, provides 20 K helium for the inner CHAFF pumping surfaces while handling a load of approximately 200 W. The cryostat is a refurbished 1950s refrigeration system that was originally designed for the transport of liquid hydrogen by Arthur D. Little, Inc. and Cambridge Corp. [Cambridge, 1952]. The ability to operate CHAFF-4 using only liquid nitrogen and the cryostat provides a cost-effective means for the evaluation of low-power thrusters without the added expense of liquid helium. Figure 7 shows the heat load curve for the cryostat at various shield temperatures. This curve represents a conservative estimate of the expected capability (75%).

F. Calculation of Optimum Cooling Tube Spacing
The cryogenic array consists of circular aluminum tubing that are welded to aluminum fins, this arrangement is shown in Figs. 2-3. To condense gases of interest, it is necessary to verify that temperature variations between the tubes are within an acceptable range (ΔT_{max} ~10 K). The spacing between tubes on the inner-shield system was selected to provide a safety factor slightly less than 2 based on heat transfer calculations. Figure 9 shows a depiction of the geometry. For a 1000 W thruster, the actual direct heat load imparted to the inner-shield system mounted on the target door is approximately 16% (160 W or ~ 4.8 W/m²). Therefore, including the safety margin the effective heat load is 9 W/m². The safety factor allows for uncertainties in fabrication consistency and other unanticipated difficulties. The distance between tubes sharing the same manifold is 0.30 m.

G. Calculation of Optimum Cryogenic Fin Spacing
The interactions between plume species and the shield system is predominantly governed by the surfaces found at the front edges of the fins and the LN_2 back panels. As the inner cooling array is made denser, its frontal edges play a progressively dominant role in backscattering processes. The opposite is true if they are made sparser. Based in part on Eq. 8, a range of acceptable values for the spacing of the fins can be made by minimizing the associated geometric term (Fig.10). As shown in Fig. 10, the optimum distance lies at about 0.038 m. As a matter of fabrication ease, the target door fins are radially arrayed with the outer edge spacing at 0.057 m and the inner edge at 0.025 m.

H. Estimate of Power Losses

An accounting of secondary heat-load loss mechanisms is necessary to assess the effective heat load capacity of the cryostat. The support for the shields is accomplished by using stainless steel caster tracks as depicted in Fig.11. Stainless steel is a relatively poor conductor and will allow for reasonably effective insulation. For a stainless steel thermal conductivity of 2 W/(mK) (@ 20 K), a contact area per caster of 4 x 10^{-5} m² and a reasonable dT/dx value of 2000 (i.e. (77-25 K)/0.0254 m), a heat loss per caster is approximately 0.2 W. With 40 casters needed to support the inner-shield system to the liquid nitrogen panels, a total heat loss due to the casters is roughly 8 W (Fig.11). In addition, although the LN_2 shields are extensive and the interior is carefully shielded, it is estimated that seams totaling 0.5% of the CHAFF 4 inside wall area will be visible to the interior. For an emissivity of 0.1 (polished stainless steel 304) and wall temperature of 300K, the associated loss due to imperfect shielding is 15 W. Table 6 summarizes the energy budget for various loss mechanisms.

I. Performance Analysis

One of the advantages of the cryogenic finned array is that it allows working panel temperatures of 20-25 K without resorting to the expensive option of liquid He. This is accomplished by having the majority of the thruster's heat load channeled to the LN_2 shield. It is necessary to estimate the thruster power that CHAFF-4 can accommodate without the use of liquid helium. It is assumed that the thruster's heat load is uniformly distributed on the target door projected area (3.7 m²). However, there is a heat load that is

Table 6: Estimated energy budget for losses within CHAFF-4.

Loss mechanisms	Energy loss (W)
Casters/support of interior helium shields	8
Seams and imperfect shielding	15
Piping losses between cryostat and CHAFF 4	5
Radiative load from LN_2 shield on CHAFF 4 interior	12
Miscellaneous	5
Total	**45**
Total wattage available for cryostat (@20K)	155

imparted to the helium fin array directly due to their finite thickness (3.175×10^{-3} m); therefore summing all the frontal areas of the finned helium array on the target door gives a total area of 0.21 m². In addition, there is another source of direct heating due to slight fin misalignment during fabrication and non-point source thruster effects. The preceding effects impact the direct heating load to the helium fins in the following manner:

$$P_{He} = P_{thruster}\left[\left(\frac{A_{frontal}}{A_{disk}}\right) + \left(\frac{A_{exposed}}{A_{disk}}\right)\{(1-\lambda)+\lambda\eta\}\right] \qquad (14)$$

where $P_{thruster}$ is the thruster's total exhaust power, $A_{frontal}$ is the frontal area due to the fin thickness (0.21 m²), A_{disk} is the projected area of the target door (3.7 m²), $A_{exposed}$ is the estimated fin area that exposed due to fabrication misalignment (0.58 m² for ±2° fin pitch angle), λ is the fraction of reflected ions and η is fraction of incident ion energy that is imparted to the fin. Equation (14) assumes that the thruster's energy is effectively transported by the ion population and is applicable for small pitch angles (i.e. ±5°) between propellant path and the normal to the edge of the target door fins. Based on computer simulations of ion/surface interaction (see next subsection), λ and η were estimated to be 0.65 and 0.50 respectively. For a 1000 W thruster, an effective heat load to the helium-finned array is roughly 160 W. Since the cryostat has approximately a 200 W heat load capability at 20 K, this design condition should be met even with the various heat load sources discussed previously (Table 6). Fig.12 shows the additional consumption of liquid helium versus thruster power for maintaining a cryopanel temperature of 20 K.

It is important to note that there is a reasonable amount of flexibility available to the operator to explore more powerful thrusters if slightly higher cryogenic panel temperatures are deemed tolerable. For example xenon pumps quite effectively below ~50 K, and its vapor pressure at 38.5 K is ~1 x 10^{-12} Torr (Fig. 13) [Garner et al, 1996 and Lide, 1992]. Consequently, thrusters with significantly greater power could still be economically tested without resorting to liquid helium (Fig. 7).

J.   Cryogenic-Array Sputter Protection Scheme

The populations of both neutrals and ions in thruster exhausts is non-trivial, the physics relating the gas-surface dynamics of these species must be used to maximize both the cryogenic shields' life expectancy and pumping efficiency.

CHAFF-4 must withstand the impact of energetic ions (~400-1000 eV), fast neutrals (~1 eV) and thermal neutrals. A xenon ion with energy of 400 eV travels at 24 km/sec. Briefly, the consequences of this bombardment are dependent on the energy of the ion, the structure and composition of the solid as well as its surface condition. The incident ion can either embed itself into the solid or scatter away from the surface. In addition, sputtered atoms are generated through energy exchange/momentum transfer processes, which are also dependent on the species participating in these interactions.

In order to determine the effect of ion flux on the various materials used in CHAFF-4, the Monte-Carlo program TRIM, which simulates energy loss and scattering mechanisms of energetic ions in amorphous solids, was used [Ziegler et al, 1985]. The impact of xenon ions with associated energies between 100-1000 eV was studied for aluminum, stainless steel, graphite and xenon. The latter is necessary since for a 5 mg/sec xenon mass flow rate, a xenon neutral atom coverage area per second is 7.5 m²/sec. At this coverage rate, a monolayer of xenon atoms would build up over the entire CHAFF-4 inner-shield array system in about 90 seconds. Since test runs will undoubtedly last on the order of a few hours, it was necessary to analyze the effect of xenon ion on xenon condensate. These test runs were also performed for impact angles of 90°, 45° and 5°. It was immediately apparent that some kind of protective material (graphite) was necessary as significant levels of sputtered material was evident for aluminum and stainless steel targets (Figs 14-17). For arcjets and resistojets, sputtering complications are second-order effects since they have low ion and neutral energies.

As shown in Figs.14-17, the greatest sputtered yield stems from xenon ions impacting xenon condensate. For various impact angles, the xenon condensate is roughly 5 times more likely to sputter than the aluminum or stainless steel surfaces. However the sputtered yield from the metals is substantial compared to carbon targets (graphite). For normal (90°) impact angles, the carbon generates roughly 2 orders of magnitude less sputtered material. The latter computational result is not in agreement with experimental measurements performed by Sovey & Patterson [1991], Carter & Colligon [1968] and Rosenberg & Wehner [1962]. As a result, we will be adopt the more conservative sputtering rates for Xe^+ ions on carbon (i.e. 0.03-0.10 per ion). For glancing impacts (5° and 45°) the carbon is approximately twice as good as the metals and this is in reasonably good agreement with the previously mentioned experimental work. However, the analysis presented in the following paragraphs will show that xenon condensate builds up on the surfaces that are near parallel to the thruster efflux for the majority of ion and Hall-effect thrusters, thereby acting as a surface protection layer. The graphite coating will greatly improve facility erosion issues for normal ion impact trajectories compared to metal surfaces.

In order to make reasonable decisions on which areas to protect with graphite, it is necessary to estimate the rates at which xenon atoms are condensed and/or sputtered on various surfaces. The two most relevant areas to consider are the edges of the fins (roughly normal to incident ions ~ 90°) and the sides of the fins which are approximately tangent (~5°) to the incident ions. The liquid nitrogen panels located at the target door as well as on half of the side panels will be covered with graphite since they will receive most ions directly with no benefit of a protective condensate layer (i.e. liquid nitrogen temperatures do not effectively pump most propellants of interest). The following relations can be used to determine

whether a viable build up of xenon atoms (in terms of protecting the aluminum fins from direct bombardment) can occur on the front edges and sides of the aluminum cryofins located at the target door area:

$$\frac{dN_{front\ edges}}{dt} = \dot{N}(1-\alpha)\Sigma_{neutrals}\Lambda - \dot{N}\alpha\Phi_{90}\Sigma_{ions} \tag{15}$$

$$\frac{dN_{sides}}{dt} \approx \dot{N}\Sigma_{neutrals}\left[\frac{1}{2}\left(1-\frac{w}{h}\right)\right]\Lambda - \dot{N}\alpha\Phi_{5}\Sigma_{ions}\sin(\theta) \tag{16}$$

where $\dot{N}$ is the propellant flow rate, Φ is the sputtering yield for different impact angles (i.e $\theta = 90°$ or $5°$), Λ is the sticking coefficient for neutral species on cryogenic surfaces and Σ is the correction for the different expansion angles from the thruster between ions and neutral species. Figs. 18-19 display the concepts for the above expressions. Analytical results are shown in Figs. 20 - 21. As exemplified in Fig. 20, there is no significant xenon condensate accumulation on the front edges of the target fins for the vast majority of propellant ionization fractions (α) and neutral concentration factors (Σ). The opposite is the case for the side impact areas (Fig. 21). The latter builds up xenon monolayers effectively for most realistic levels of propellant ionization fractions and impact angles (θ). Consequently, the front edges of the aluminum cryogenic fins will have thin graphite layers bonded to them for sputtering protection, whereas the sides will not.

It is necessary to estimate the graphite thickness needed to both protect the aluminum and allow reasonable heat conduction. From Fig.14, the sputtered percentage of carbon atoms (from graphite coating) due to xenon ion impact is roughly 0.2% of incident fluxes (90°). However, based on previous experimental work by Sovey & Patterson [1991], the sputtered yield should be between 0.03-0.10 per ion. Following a conservative approach (assume 10% sputtering rates), the erosion rate of graphite due to xenon ions (at 1000eV) is roughly 1×10^{-10} meters of carbon sputtered per second (at 5 mg/sec Xe flow rates over a projected area of 3.7 m²). Hence a graphite layer that is 20 mils thick (5×10^{-4} m) would last approximately 1400 hours. This estimate is surprisingly long given qualitative discussions with facility operators who witness noticeable changes after a few tens of hours of operation [Goodfellow, 1997]. In any event, since no xenon condensate is likely at the leading edges for ion and Hall-effect thrusters, the graphite can be somewhat thicker since heat transfer is not as critical. However, the leading edges can condense much of the propellant fragments for arcjet and resistojet thrusters. Therefore, an optimum thickness of graphite should be adopted that allows both effective heat transfer (maintain a $\Delta T \approx 3$ K between the graphite and aluminum) and extends its useful life. Based on the heat-transfer specifications of graphite (~ 0.03 W/(mK) @ 20 K) [Ho et al, 1968], a thickness 0.8 mm (~ 30 mils) was adopted as an initial covering.

In addition, it is relevant to consider the fate of those xenon ions that imbed themselves into the graphite layers since these may or may not diffuse out from the graphite lattice and add to the level of background gas in the facility. Based on the TRIM code results, it is evident that for the energies of interest (100-1000 eV), the penetration depth of xenon ions into carbon varies between 5 and 35 Å. Hence, these ions are considered to stop relatively close to the surface of the carbon (within 7 monolayers). Consequently, if the physical bond strength between xenon and carbon can be estimated, it would be possible to approximate the associated residence time and determine whether implanted ions need to be considered as potential complicating factors for the duration of most tests. An analysis is presented in the following paragraphs discussing the approach.

By using the approach outlined in Shemansky [1997], the following relations can approximate the lifetime that physical or chemical bonds have when fighting against thermal dissociation:

$$\tau = \tau_0 \exp\left(\frac{D_0}{kT}\right) \qquad (17)$$

where τ_0 is the fundamental period of the vibrating molecule, D_0 is the dissociation energy, k is the boltzman constant and T is the temperature (K). It is necessary to obtain reasonable estimates of τ_0 and D_0 so as to determine an appropriate molecular bond lifetime.

First, an estimate of D_0 can be determined from the following expression:

$$D_0 = D_e - \frac{1}{2}\omega_e + \frac{1}{4}\omega_e \chi_e \qquad (18)$$

where D_e is the energy depth between the lowest vibrational level (v=0) to the dissociation limit, ω_e and $\omega_e\chi_e$ are the vibrational energy and the distortion constants expressed in energy units of cm^{-1}. The fundamental period τ_0 can be derived from the following expression:

$$\tau_0 = \frac{1}{c(\omega_e - \omega_e\chi_e)} \qquad (19)$$

The spectroscopic constants ω_e and $\omega_e\chi_e$ were determined to be 121.50 cm^{-1} and 3.53 cm^{-1} respectively. For these values, the parameter D_0 is ~ 1.97 x 10^{-13} ergs and τ_0 was calculated to be 2.83 x 10^{-13} s. Eq (16) is plotted in Fig.22 and shows that the effective lifetime of the Xe-C bond is quite short (~10 μs) at liquid nitrogen temperatures and longer than the projected tests at 35 K or below. Hence we expect that all xenon species (ions and neutrals) will readily reflect and/or diffuse from the graphite shield on the liquid nitrogen back panel (i.e. sticking coefficient = 0) whereas the xenon ions will remain embedded in the carbon lattice located at the front edges of the inner cryo shield.

K. CHAFF-4 Pumping Speed

Based on the content of the previous subsections and the earlier discussion of background number density in Sec. II, the CHAFF-4 pumping speed can be estimated. The cryosurface design for CHAFF-4 has two configurations as illustrated in Figs 4a-b for the forward and backflow regions of the facility. Their respective location in the facility is indicated in Fig. 2. For the forward flow segment the design is dictated by the necessity to shield the inner cryosurface (~20 K) from energetic thruster ions. The geometry allows the majority of the plume species to flow tangentially past the inner finned array and impact the LN_2 outer shield. Since there is a significant errosive issue due to xenon ions impacting an aluminum surface, a graphite layer was introduced to protect the LN_2 shield. It would be advantageous to have the graphite layer act as a cryosorption pump with respect to incoming ions. Unfortunately, based on the TRIM code results, at normal thruster energies xenon ions tend to penetrate about 2 monolayers deep in the graphite. From the result discussed in the previous sub-section, which is summarized in Fig. 22, the lifetime of a xenon-carbon physical bond at 77 K is too short (~10 μs). Consequently any absorbed/adsorbed xenon atom would very likely desorb on a timescale of a few tens of μsec. However, since the residence time of xenon in the lattice depends, in part, on the actual penetration distance and subsequent damage within the column depth traced out by the trajectory of the xenon atom within the graphite, it cannot be concluded a priori that all xenon atoms/ions will quickly desorb after a brief physical bond with the graphite surface/subsurface. Therefore, Fig. 8 displays the expected background number densities for the two limiting fates of the xenon propellant ions.

It also appears that even if a xenon condensate could form, the ion bombardment would effectively sputter this layer away for most propellant ionization fractions (Fig. 20). The LN_2 shield is a mandatory component since it insolates the inner cryofin system from the ambient thermal heat load (~ 300 K). Regretably, the forward LN_2 shield surface (graphite) becomes a major source of backscattered atoms in the chamber's interior. It is interesting to note that for relatively low energy (few hundred K) neutrals

typical of ion thrusters the configuration indicated in Fig. 4(b) would give a pumping speed per unit projected area (the surface defined by the leading edge of the fins) up to fifty times the pumping speed of the Fig. 4(a) configuration.

Using the present configuration of the CHAFF-4 cryoshields consider the representative background number density in the chamber $(n_{BS})_{C,i}$ given by eqs (10) and (11). It is expected that both xenon neutrals and ions will essentially accommodate to the graphite surface and leave with the same energy. The backscattered number density can therefore be calculated using the incident xenon mass flow (i=N):

$$(n_{BS})_{C,N} = \frac{(1-\alpha_i)\dot{M}_{EX}(F_{BS})_{C,N}}{m_n \overline{V}_N A_C} \tag{20}$$

where α_i is the ionization fraction of the exhaust gas and is 0 for the case where ions are not trapped by the graphite, $\overline{V}_N$ is the mean thermal speed of the xenon neutrals assuming they are fully accomodated to the graphite surface temperature of 77 K and A_C is the cross sectional area of the volume inside the cryoshield and normal to the longitudinal axis of the facility (5 m²).

The total backscatter number densities and equivalent altitudes (sputter plus neutrals) are plotted in Fig. 8 as a fraction of α_i for a range of $\dot{M}_{EX}$. Fig. 8 shows a range of possible background number densities, which depends on the fate of the inbound xenon ions. The bottom curve represents the expected background number density if the ions are trapped in the graphite lattice. The top curve (mostly straight) shows the outcome if the xenon atoms diffuse back out from the graphite sublayers. The pumping speed is estimated to be 9×10^6 l/sec. CHAFF-4 has about 30-40 times lower density than a comparably sized (moderate) conventional facility and a 3 to 4 times lower density than a large conventional facility.

L. Sting Design
It is anticipated that the elapsed time during which diagnostic data is secured will typically extend for several hours. Therefore, it is paramount that flexibility be incorporated in CHAFF-4 to maximize data quality and quantity during limited operational test times. A hydraulically actuated sting, shown in Fig. 23, is incorporated in CHAFF-4 on which various thruster types may be secured. The sting allows longitudinal translations (±1 m) of the thruster with a projected accuracy of ±5 mm. Three-dimensional optical diagnostic surveys are accomplished by utilizing a cryogenic temperature resistant stepper motor system attached to the sting. The latter consists of one rotation and two translation axes (±15 cm). The flexibility of this system greatly enhances scientific productivity during limited test times since a complete three-dimensional survey can be performed of the plume environment.

The sting arm itself is shrouded in a liquid nitrogen cooled outer skin to minimize the adverse heat load on the inner cryogenic shield system. The shroud system also allows for the radiative isolation of the rear and side quadrants of various thrusters further reducing adverse heating of the helium-cooled inner-shield system.

Various feedthroughs designed for fiber optics, LN₂, power and gas requirements are incorporated at the end flanges of the sting. The respective cabling/tubing is positioned inside the sting with enough excess length outside to allow uninterrupted service as the sting is actuated during a test.

Finally, there is a contingency for floating the thruster potential relative to ground in order to investigate the effect of spacecraft charging on operating and plume characteristics.

VI. Construction of CHAFF-4
Based on the design considerations presented in the previous sections, the CHAFF-4 vacuum envelope was ordered from Howard Fabrication, Industry, CA in September 1997 and delivered in July 1998. Two

1 m diffusion pumps (Zyrianka 900) were ordered from the Experimental Scientific Technological and Educational Center, Novosibirsk, Russia. The first was delivered in March 1998 and the most recent in December 1998. From June to November 1998 on-site construction of the LN2 cryoshields and gaseous helium pumping surfaces took place, with the considerable amount of aluminum welding accomplished by Lloyd's Welding, Redondo Beach, CA. During this period the backing line plumbing was also installed and connections made with the backing pumps that were already available (see Fig. 1).

Several photographs shown in Figs 24-27 illustrate the interior and exterior of the CHAFF-4 as it is currently configured for detailed leak checks and subsequent performance tests.

VII. Conclusions

Design objectives for the CHAFF-4 contamination and plume diagnostic facility have been outlined. The need to perform plume studies and obtain contamination footprints drove CHAFF-4 designers to pursue a unique approach with respect to cryogenic pumping than is traditionally used. Development of an extensive multi-finned cryogenic shield system (590 m² maintained between 20-35 K) results in significantly lower background densities than is typically found in facilities of this kind (with lower limits between 5×10^{14} and 4×10^{15} m^{-3}). Equivalent test altitudes ranging between 150-350 km are possible depending on thruster operational specifications. The pumping speed expected for an ion thruster (with xenon mass flow rate of 5 mg/sec) is 9×10^6 l/sec. The facility is cooled by a cryostat system that enables the testing of a range of thrusters, up to a power level of approximately 3500 W, without resorting to supplementary liquid helium. In addition, it is possible to introduce liquid helium for those occasions when it is warranted. An analysis to protect the facility against ion-driven sputtering erosion resulted in the use of appropriately positioned graphite layers.

It will be necessary in the near future to perform detailed shakedown and performance tests to establish the actual performance envelope of CHAFF-4 and to validate the design principles. Finally, the greater goal for the David P. Weaver Collaborative High-Altitude Flow Facility is to develop a detailed understanding of the complications and/or advantages inherently found in this type of facility, and to develop possibly more effective approaches for investigating space propulsion systems.

Acknowledgements

References

Banks, B., private communications.

Brown, R.F., Heald Jr., J.H., "Background gas scattering and skimmer interaction studies using a cryogenically pumped molecular beam generator", Fifth International Symposium of Rarefied Gas Dynamics, 2, 1967.

Bütefisch, K.A., and Koppenwallner, G., "An orbital research facility for rarefied, reactive, and plasma flows", Presented as invited lecture G at the 11th International Symposium on Rarefied Gas Dynamics, Cannes, July 3-8, 1978.

Caledonia, G., Krech, R., and Green, B., "A high flux source of energetic oxygen atoms for material degradation studies", AIAA Journal, 25 (1), pp. 59-63, 1987.

Cambridge, Operating Manual for Refrigerated Transport Dewar. Cambridge Corp. Sept. 1952.

Carter, G., Colligon, J. S., Ion Bombardment of Solids, American Elsevier, New York, 1968.

Dettleff, G. and Plahn, K. "Initial experimental results from the new DLR-high vacuum plume test facility STG", AIAA 97-3297, 1997.

Dettleff, Georg., "Plume flow and plume impingement in space technology", Prog. Aerospace Sci., 28, PP. 1-71, 1991.

Filliben, F.D. Electric Propulsion for Spacecraft Applications. Chemical Propulsion Technical Reviews 96-64. December, 1996.

Filliben, J.D. Electric Thruster Systems. Chemical Propulsion Technical Reviews 97-65. June, 1997.

Garner, Charles E., Brophy, John R., Pless, L.C., Barnett, John W., "The effect of nitrogen on xenon ion engine erosion", AIAA 90-2591, 21st International Electric Propulsion Conference, Orlando, Florida, 1990.

Garner, Charles E., Polk, James R., Brophy, John R., Goodfellow, Keith., "Methods for cryopumping xenon", AIAA 96-3206, 1996.

Goodfellow, K., private communications, 1997.

Hechtl, E., Bohdansky, J., "Sputtering behavior of graphite and molybdenum at low bombarding energies", Journal of Nuclear Materials, 123, pp. 1431-1436, 1984.

Ho, C.Y., Powell, R.W., and Liley, P.E., "Thermal conductivity of selected materials: Part 2", NSRDS-NBS 16, pp. 82-133, 1968.

Hufenbach, B., Dettleff, G., Böttcher, R. D., Trinks, H., Cheox-Damas, P., Theroude, C., Castegon, S., "European activities in plume testing", AIAA-97-3301, 33rd Joint Propulsion Conference and Exhibit, Seattle, Washington, July 1997.

Hughes, http://www.hughespace.com/hsc_pressreleases/98_01_14_edd.html/, 1998.

Iliasova, N., Nedosekova, S., Rebrov, A., Skovorodko, P., and Roig, J., "Computational optimization of diffusion pump parameters", Vacuum, 55 (5-7), pp. 745-747, 1993.

Ivanov, M.S., Markelov, G.N., Gerasimov, Yu.I., Krylov, A.N., Mishina, L.V., Sokolov, E.I., "Free-flight experiment and numerical simulation for cold thruster plumes", AIAA 98-0898, 36th Aerospace Sciences Meeting & Exhibit, Reno, NV, 1998.

Ketsdever, A., "The production of energetic atomic beams via charge exchange for the simulation of the low-Earth orbit environment", Ph.D. Dissertation, University of Southern California, 1995.

Ketsdever, A., Weaver, D., Muntz, E.P., "A facility to produce an energetic, ground state atomic oxygen beam for the simulation of the low-Earth orbit environment", NASA Conference Publication 3280, pp. 121-138, 1994.

Lebéhot, A., Campargue, R., "Electronic relaxation in laser sustained argon and argon-oxygen plasma free jets", Rarefied Gas Dynamics 20, p.757, Peking University Press, Beijing, 1997.

Lide, D. R., <u>CRC Handbook of Chemistry and Physics</u>, CRC Press, Boca Raton, Florida, 1992.

McLean, C. H., Lesky, O., "Development of a helium cryopumped facility to evaluate Hall Effect Thrusters", IEPC-97-135, 25th International Electric Propulsion Conference, Cleveland, Ohio, August 1997.

Meyer, J.-Th., "Cryogenic pumping speed for a freejet in the scattering regime," Progress in Astronautics and Aeronautics, Rarefied Gas Dynamics: Physical Phenomena, 114, pp. 218-233, 1989.

Moore, J. H., Davis, C.C., Coplan, M.A., <u>Building Scientific Apparatus - 2nd Ed.</u>, Addison-Wesley Publishing Company, Reading, Massachusetts, 1989.

Mueller, J. "Thruster options for microspacecraft: a review and evaluation of existing hardware and emerging technologies", 33rd Joint Propulsion Conf., AIAA 97-3058, July, 1997.

Muntz, , E.P., Hamel, B.B., Maguire, B.L., "Some characteristics of exhaust plume rarefaction", AIAA Journal, 8, pp. 1651-1658, 1970.

Nanbu, K., Watanabe, Y., Igarashi, S., Detleff, G., Koppenwallner, G., "Effectiveness of a parallel plate arrangement as a cryogenic pumping surface", Progress in Aeronautics and Astronautics, Vol. 117, p. 233-243, 1988.

Orient, O., Chutjian, A., Murad, E., "Recombination reactions of 5-eV O(3P) atoms on a MgF2 surface", Phys. Rev. A, 41 (7), pp. 4106-4108, 1990.

Randolph, T., Day, M., Kim, V., Kaufman, H., Zhurin, V., Kozubsky, K., "Facility effects on SPT thruster testing", IEPC-93-093, 23rd International Electric Propulsion Conference, Seattle, Washington, September 1993.

Rebrov, A., " Proceedings of the 15th International Symposium on Rarefied Gas Dynamics", Grado, Italy, pp. 455-473, 1986.

Rebrov, A.K., "Gasdynamic and thermophysical optimization of the jet vacuum pumps", Vuoto, 20 (2), pp. 288-293, 1990.

Rosenberg, D., Wehner, G. K., "Sputtering yields for low-energy He$^+$, Kr$^+$, and Xe$^+$ ion bombardment", Journal of Applied Physics, Vol.33, No. 5, pp. 1842-1845, May 1962.

Shemansky, D. E., AE-587 Gas-Surface-Interactions, class notes, 1997.

Simpson, H.B., Wallace, N.C., "The lifetest of UK-10 ion thruster cathodes and neutralizers: implications for facility design", ESA SP-398, Aug., 1997.

Sovey, J. S., Patterson, M. J., "Ion beam sputtering in electric propulsion facilities", AIAA-91-2177, 27th Joint Propulsion Conference, Sacramento, California, 1991.

Stephens, J. P., "Space molecular sink simulator facility design", JPL Technical Report No. 32-901, March 1966.

Vaghjiani, G., "Discharge flow-tube studies of O(3P)+N2H4 reaction", J. Chem. Phys., 104 (14), pp. 5479-5489, 1996.

Van Zyl, B., Gealy, M., "New molecular-dissociation furnace for H and O atom sources", Rev. Sci. Instrum., 57 (3), pp. 359-364, 1986.

Varian, Varian Vacuum Products 1997-1998 Catalog, Varian Associates, Inc., Leington, Massachusetts, 1997.

Wang, J. and Brophy, J., "3-D Monte-Carlo Particle-in-Cell simulations of ion thruster plasma interactions", AIAA 95-2826, San Diego, CA, July 1995.

Wehner, G. K., "Influence of angle of incidence on sputtering yields", J. App. Phys., 30 (11), pp. 1762-1765, November 1995.

Wood, B.E., Hall, D.F., Lesho, J.C., Boies, M.T., Silver, D.M., Uy, O.M., Benson, R.C., Dyer, J.S., Galica, G.E., Green, B.D., Bertrand, W.T., "MSX satellite: flight measurements of contaminant films", AIAA 98-2592, 7th AIAA/ASME Joint Thermophysics and Heat Transfer Conference, Albuquerque, NM, 1998.

Würsching, C., "Residual gas analysis in a space simulation facility", Vacuum, 43, (1,2) pp. 137-141, 1992.

Ziegler, J.F., Bierback, J.P., Littmark, U., The Stopping Range of Ions in Solids, Pergamon Press, New York, 1985.
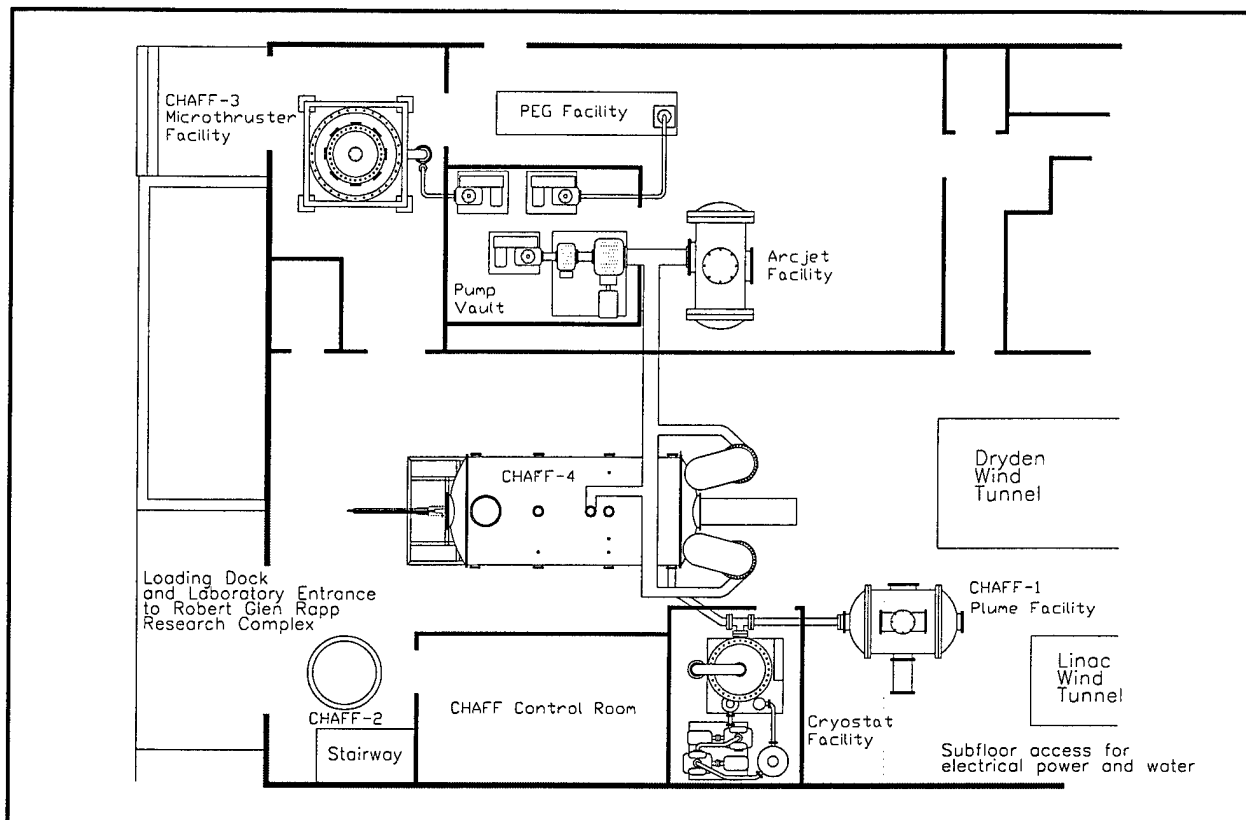
Figure 1: Layout of the David P. Weaver Collaborative High Altitude Flow Facility at USC.
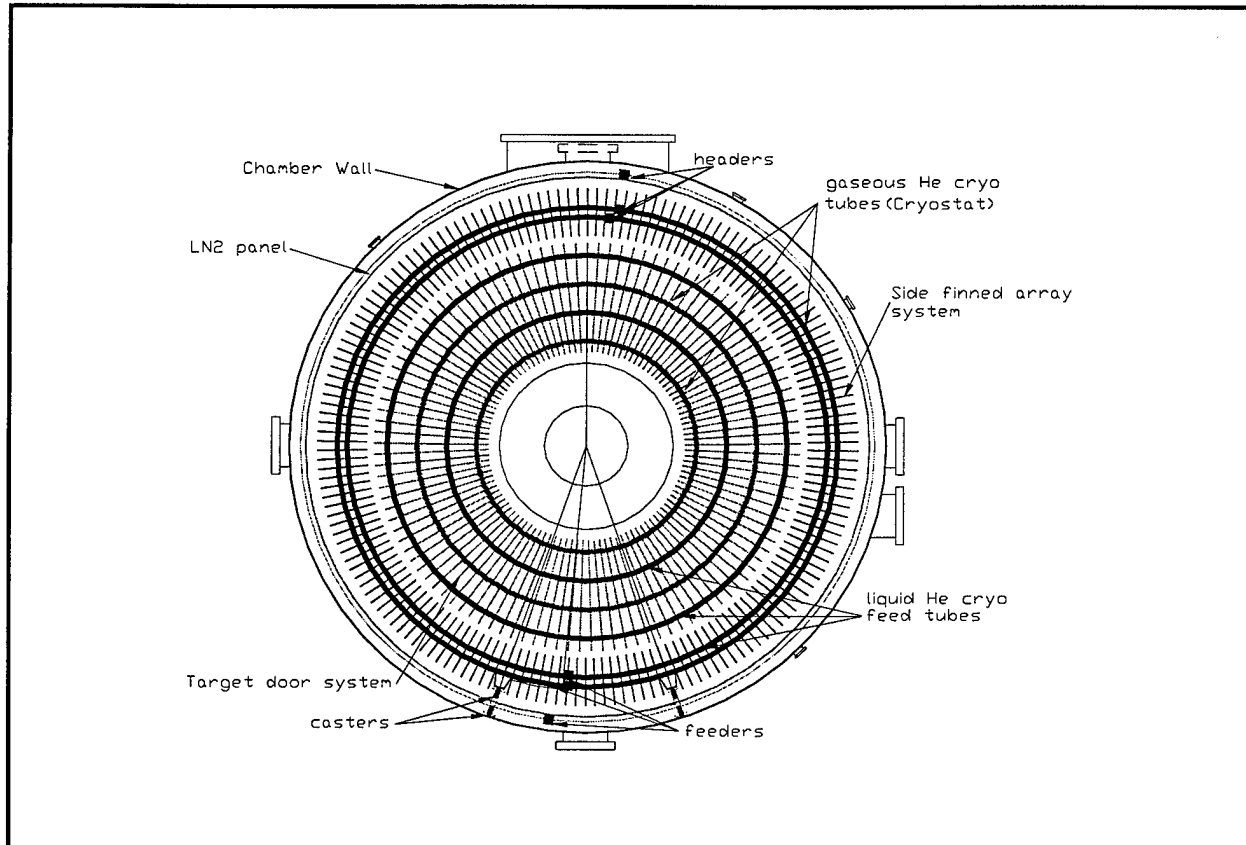
Figure 2: Front view of CHAFF-4 cryogenic array system.
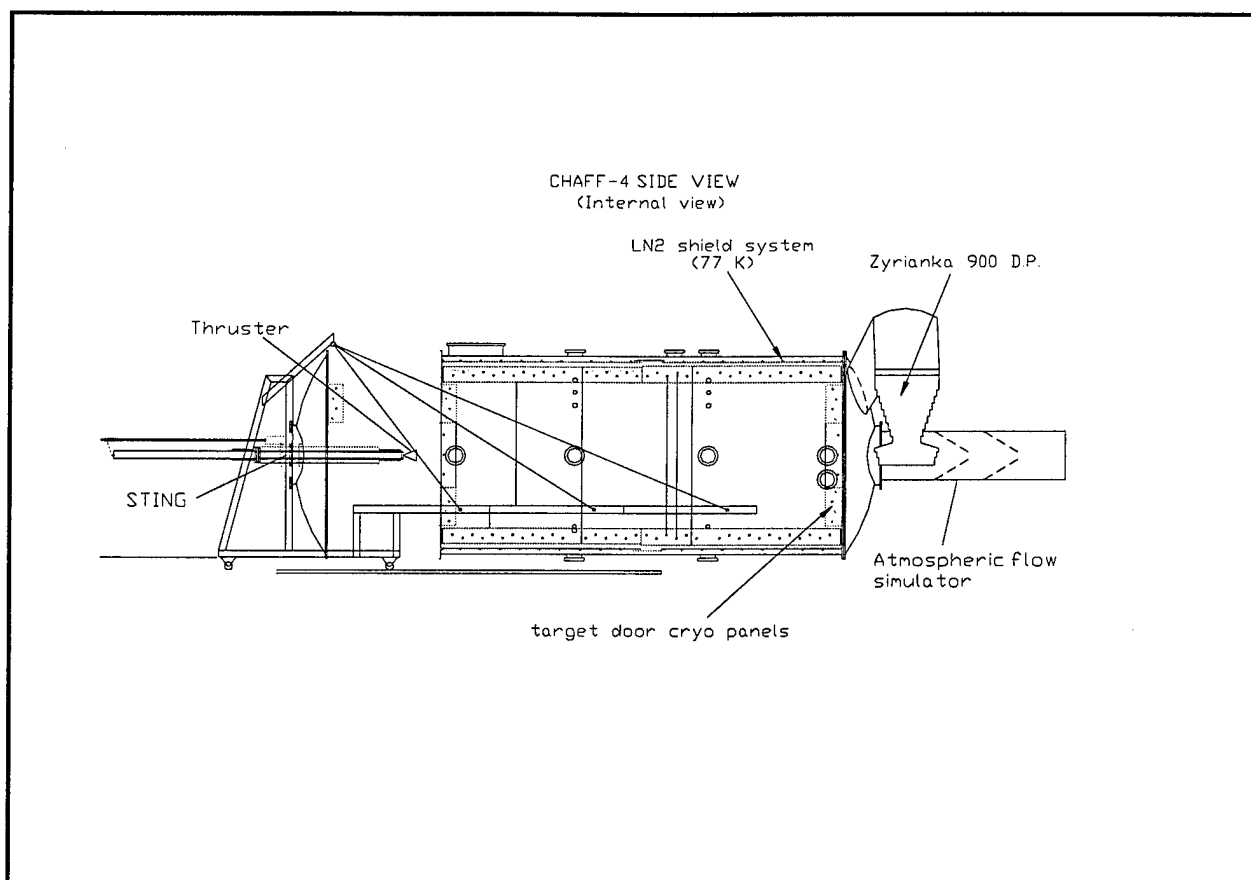
Figure 3: Side view of CHAFF-4 cryogenic system, STING apparatus and atmospheric flow simulator.
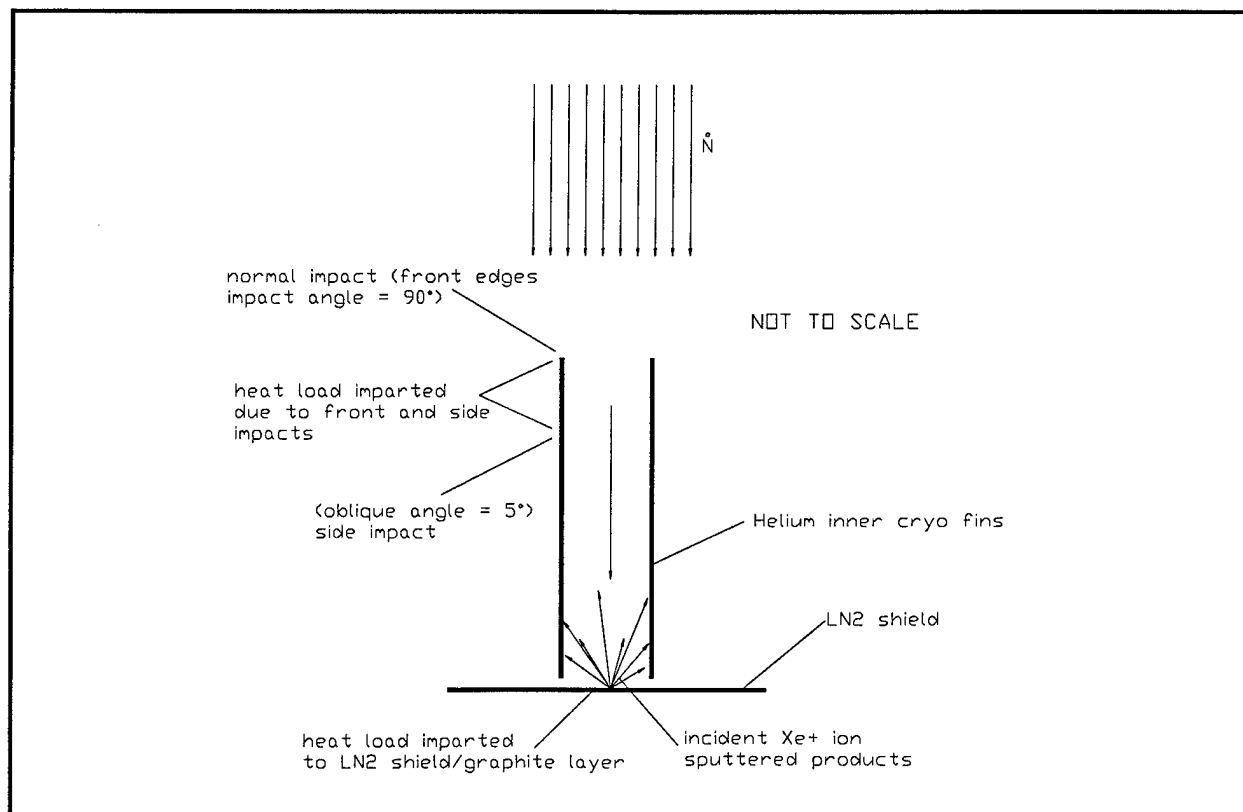
Figure 4a: Sketch of inner cryogenic shield geometry of the target door under ion bombardment.
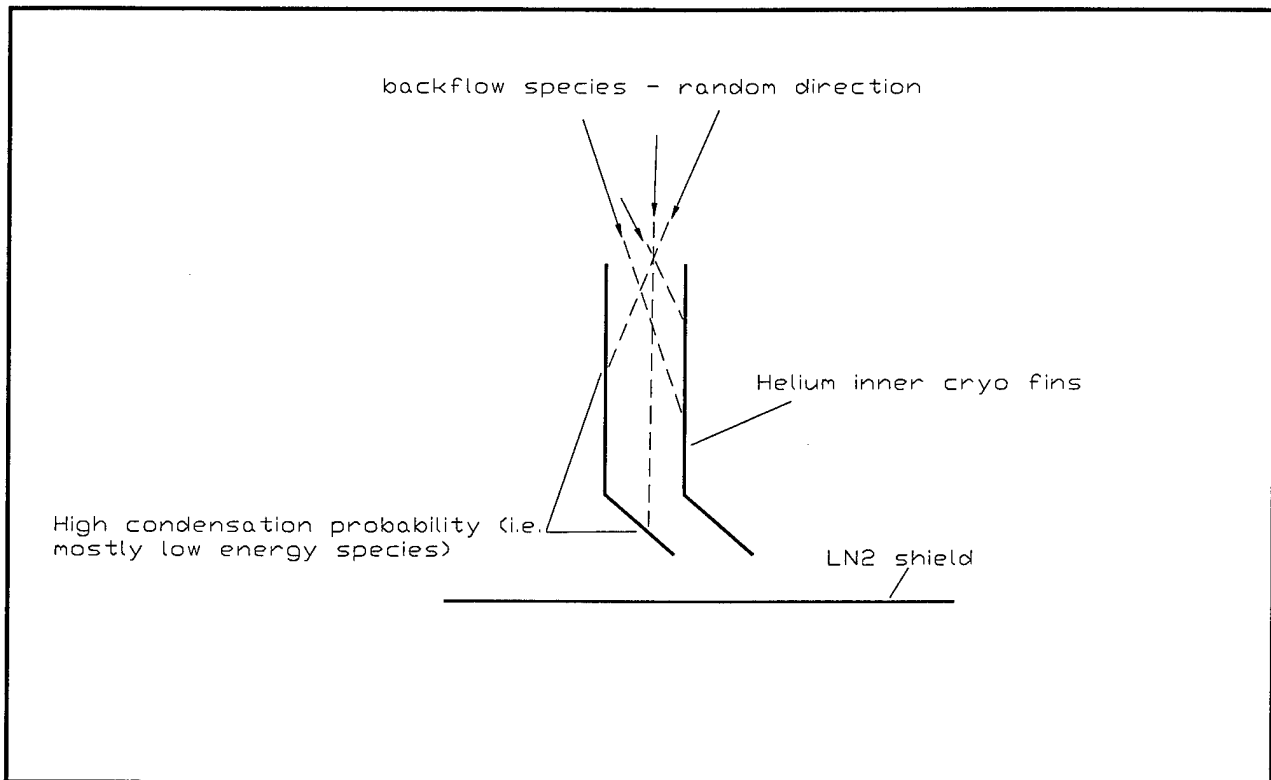
Figure 4b: Sketch of inner cryogenic shield geometry of the backflow region.
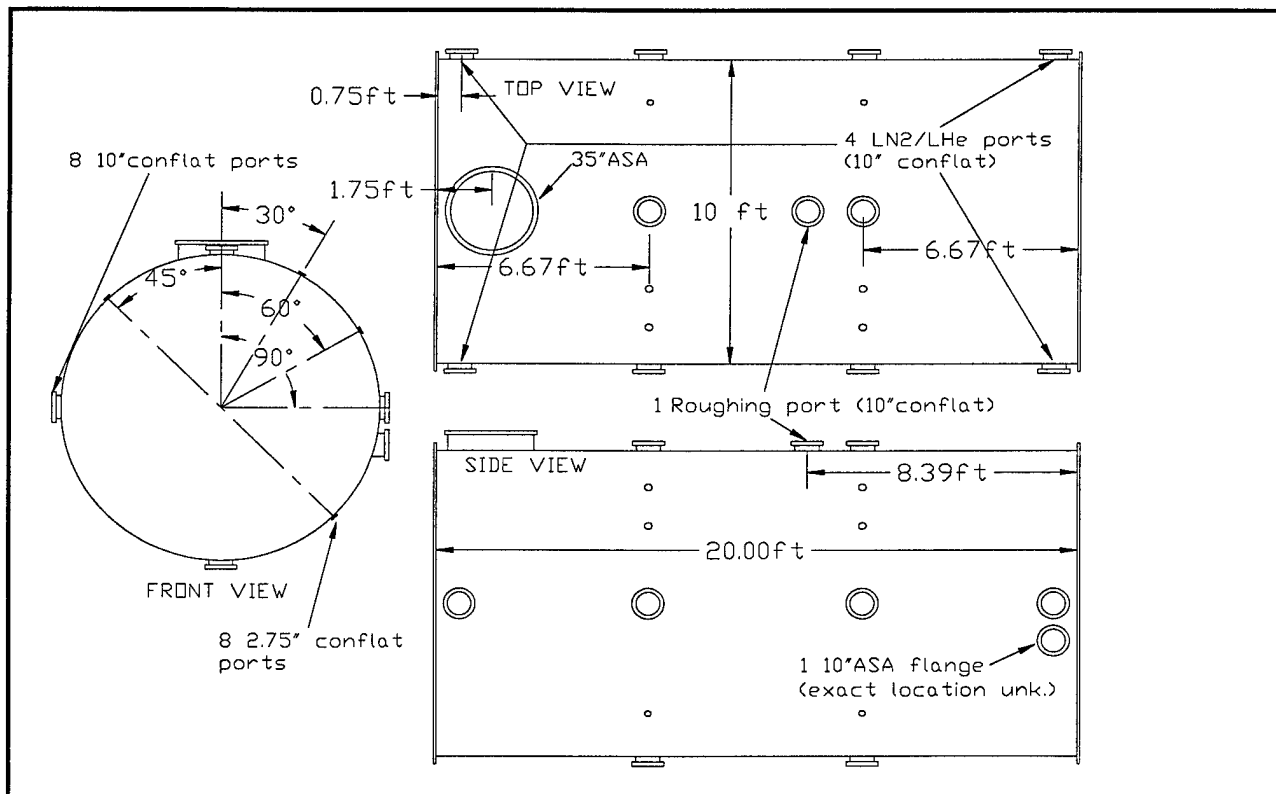
Figure 5: CHAFF-4 dimensions and chamber optical access.
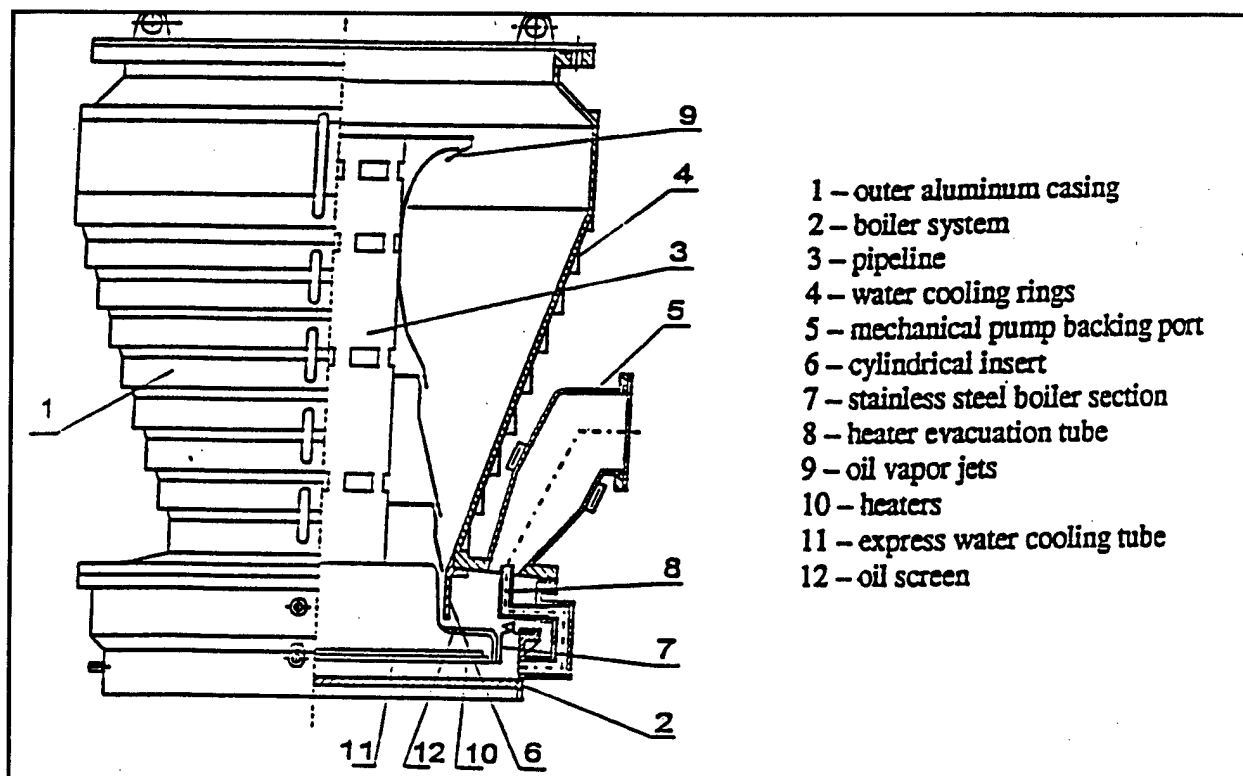
Figure 6: Zyrianka 900 diffusion pump schematic.

1 – outer aluminum casing
2 – boiler system
3 – pipeline
4 – water cooling rings
5 – mechanical pump backing port
6 – cylindrical insert
7 – stainless steel boiler section
8 – heater evacuation tube
9 – oil vapor jets
10 – heaters
11 – express water cooling tube
12 – oil screen
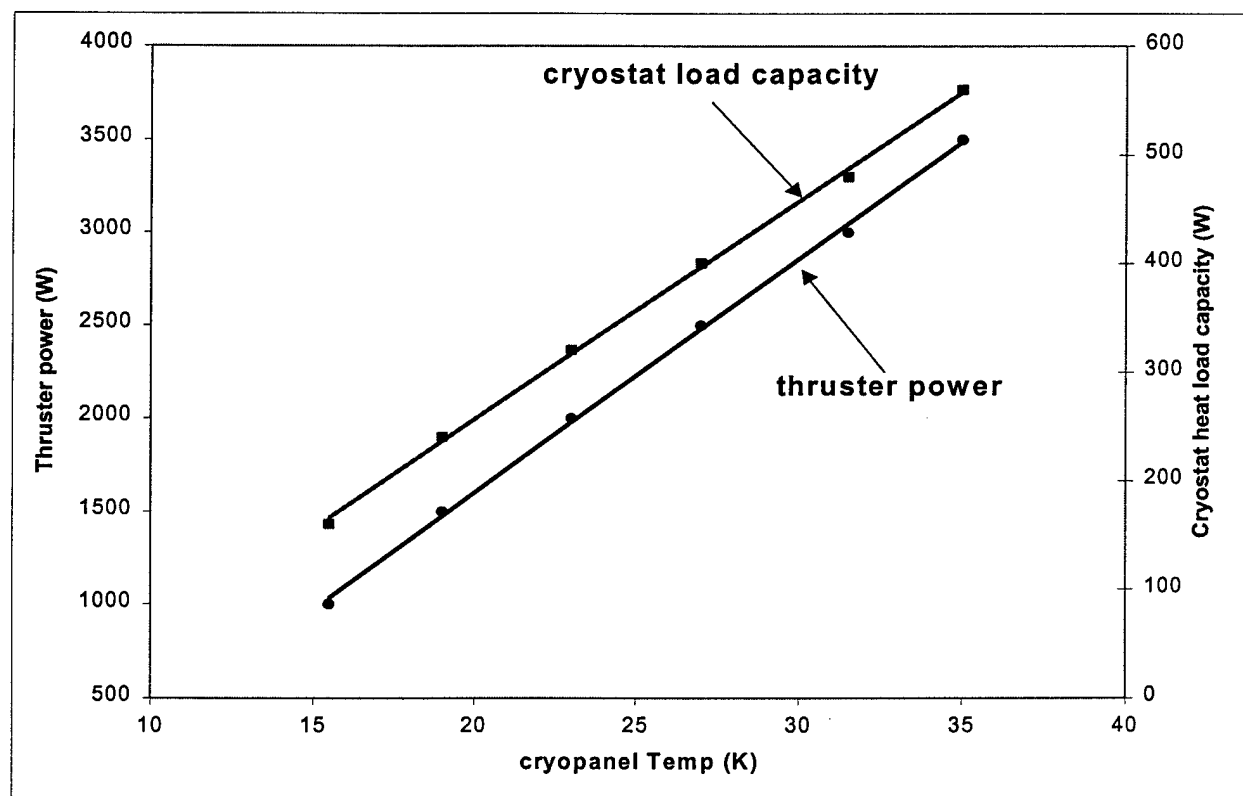
Figure 7: Heat load characteristics of CHAFF-4's cryostat vs inner shield array temperature.

Background Number Density at Vicinity of Thruster due to Backscattered Atoms
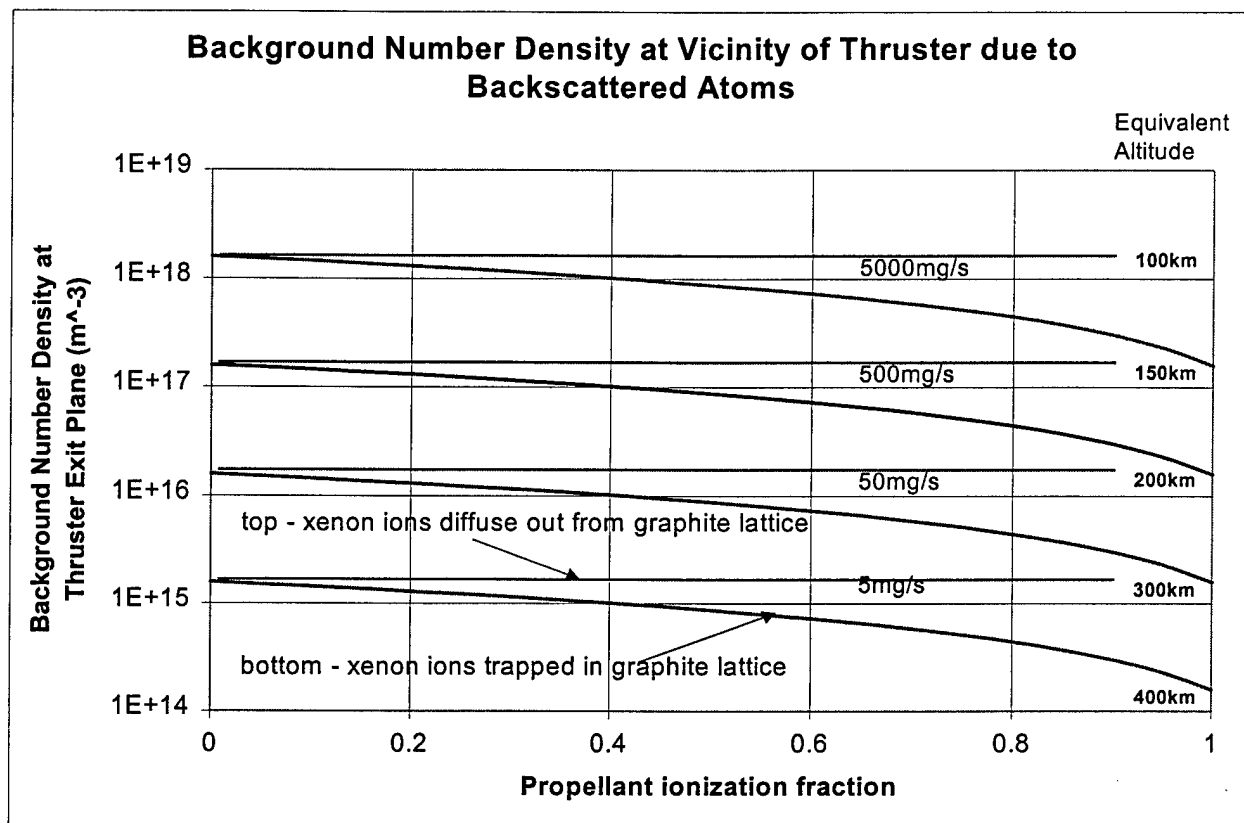
Figure 8: Background density and equivalent altitude capability versus propellant ionization fraction.
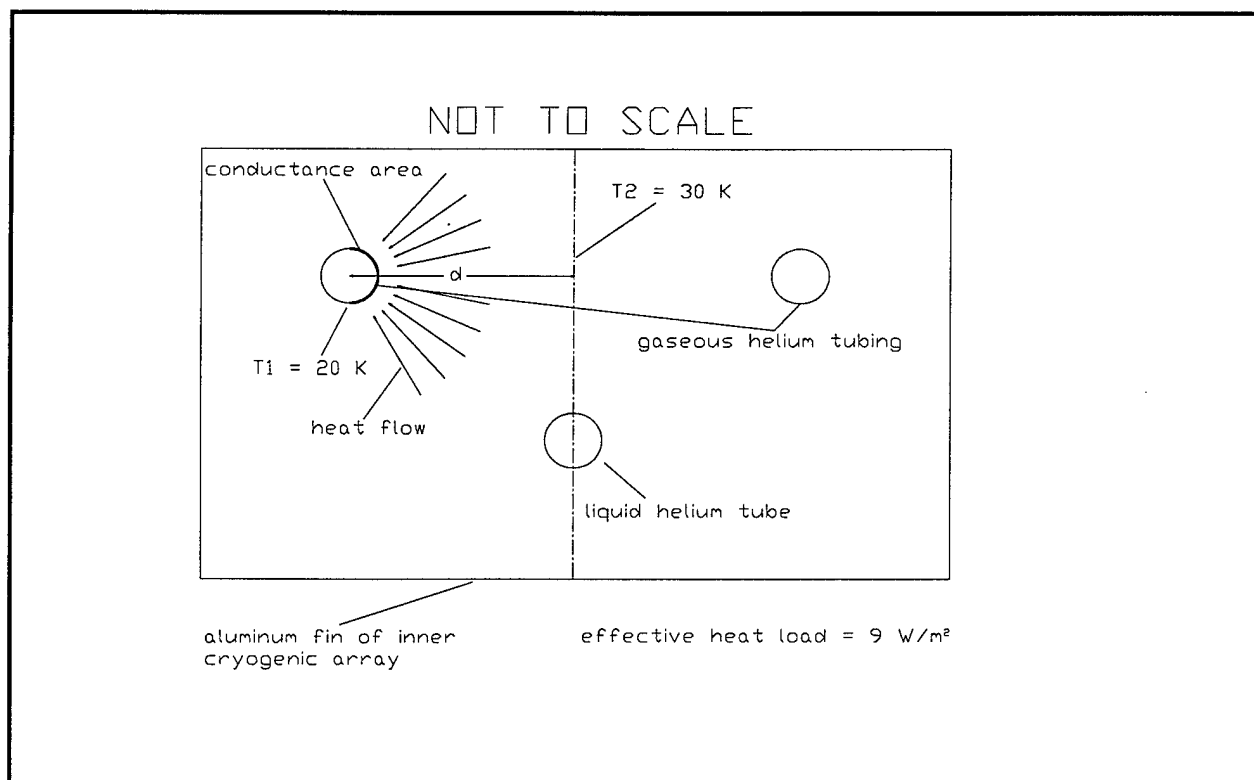
Figure 9: Cryogenic fin schematic showing heat conductance path for effective $\Delta T = 10$ K.
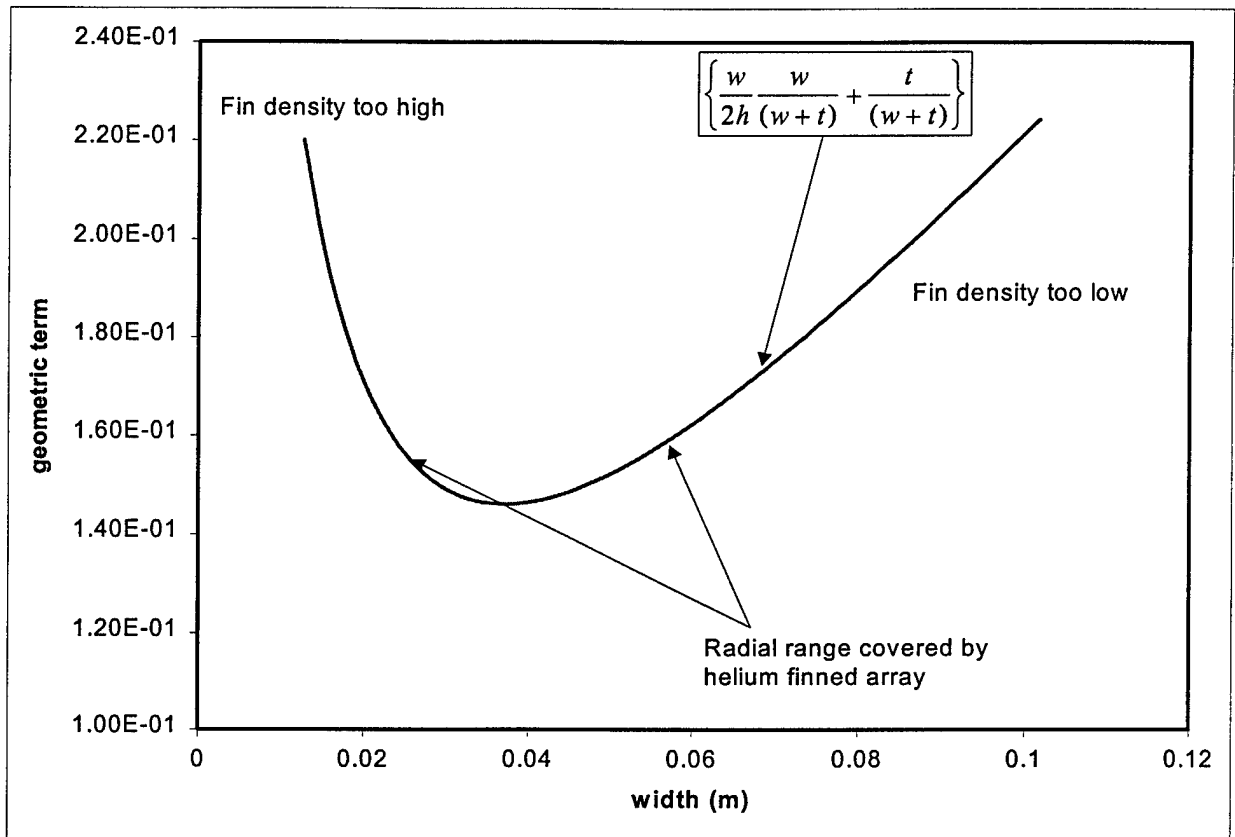
Figure 10: Optimization of fin spacing for target door shield array.

The geometric term plotted is:

$$\left\{ \frac{w}{2h} \frac{w}{(w+t)} + \frac{t}{(w+t)} \right\}$$

Labels on the plot: Fin density too high; Fin density too low; Radial range covered by helium finned array.
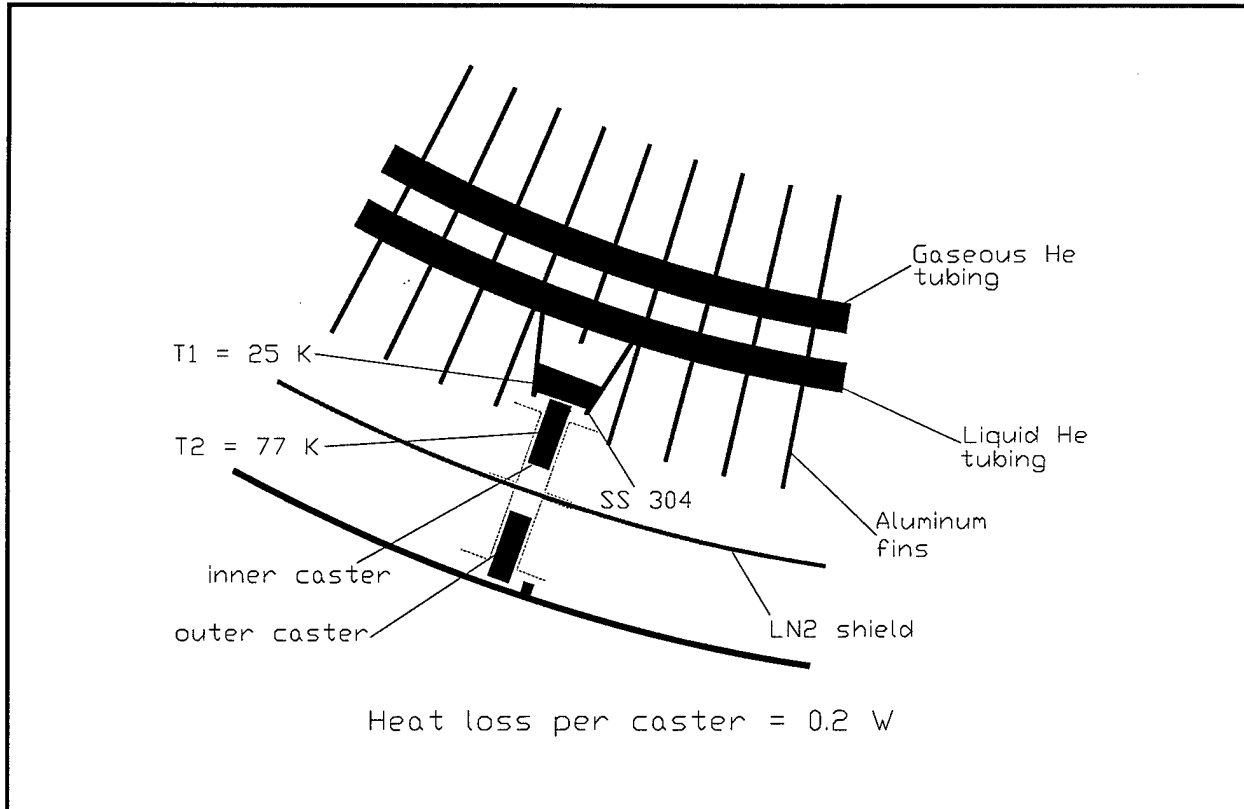
Figure 11: Heat transfer path schematic between inner cryogenic array and LN$_2$ shield.

Labels on schematic: Gaseous He tubing; Liquid He tubing; Aluminum fins; LN2 shield; SS 304; $T1 = 25$ K; $T2 = 77$ K; inner caster; outer caster; Heat loss per caster = 0.2 W
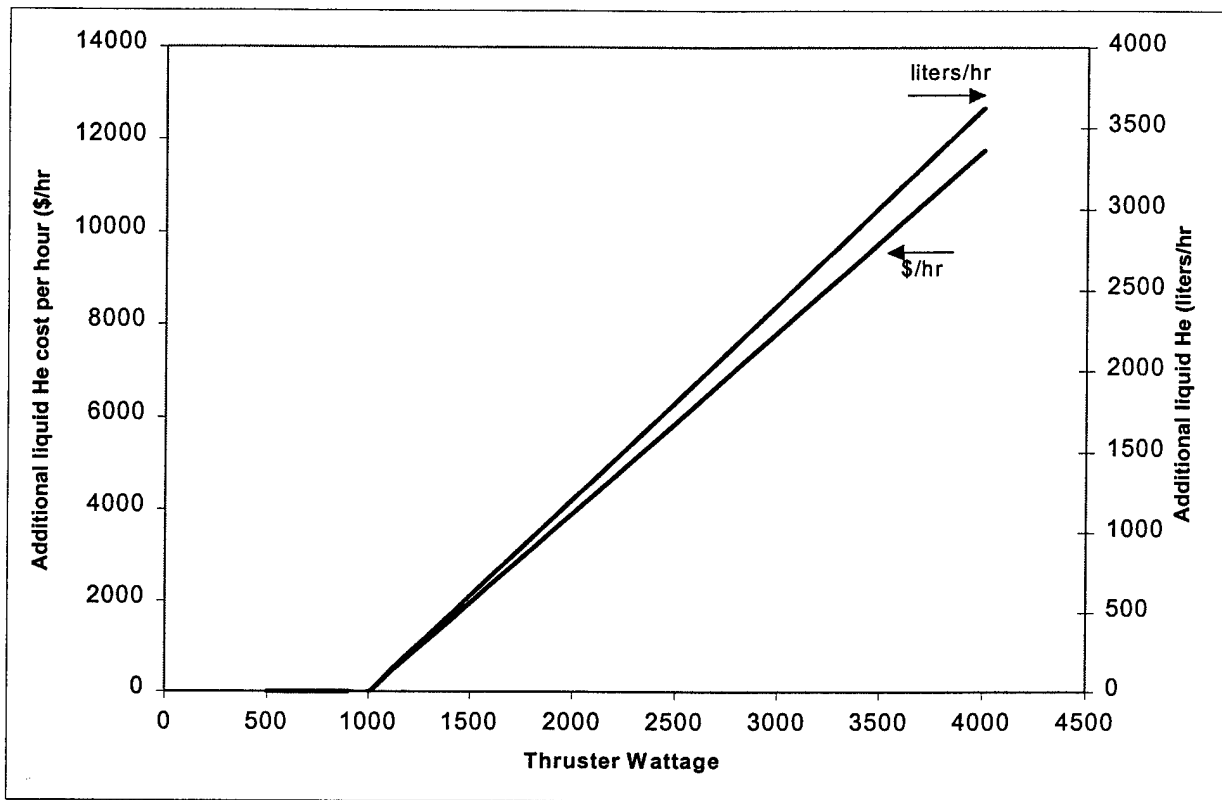
Figure 12: Liquid helium utilization vs thruster wattage needed to maintain shields at 20 K.
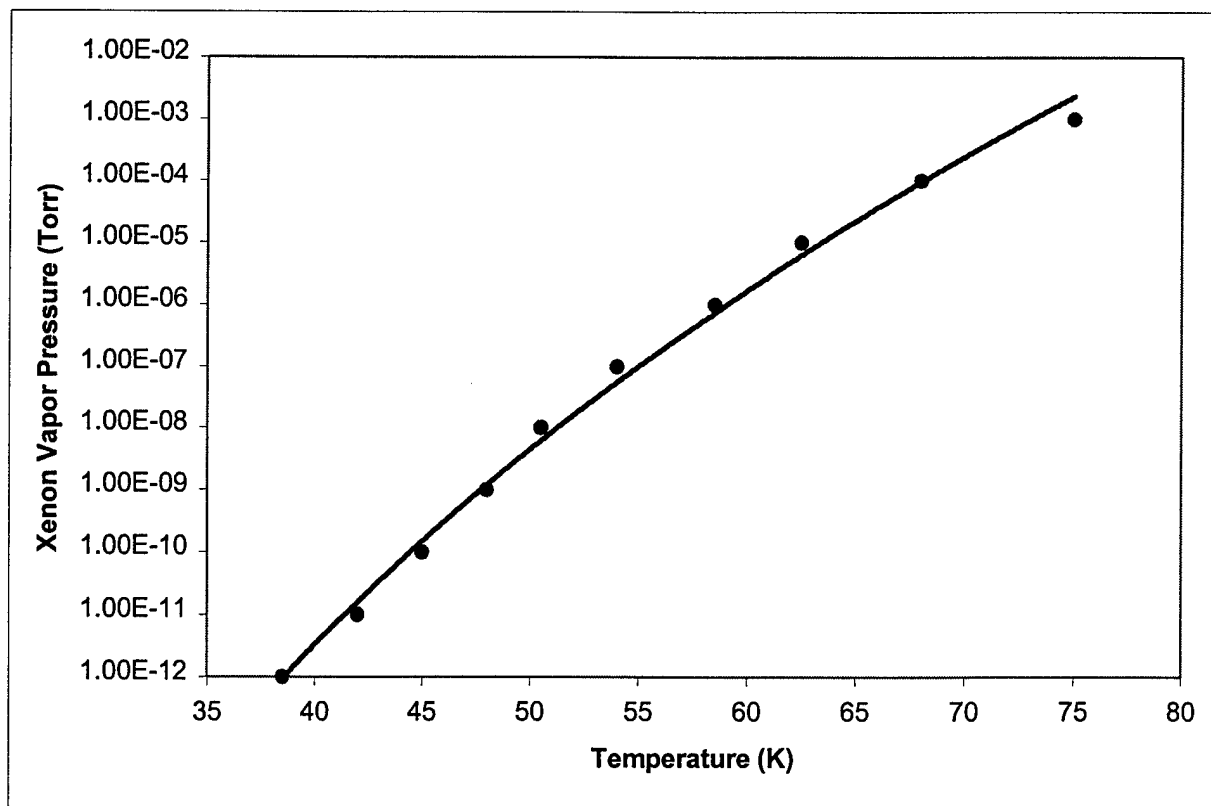
Figure 13: Xenon vapor pressure (Torr) taken from Garner et al [1996].
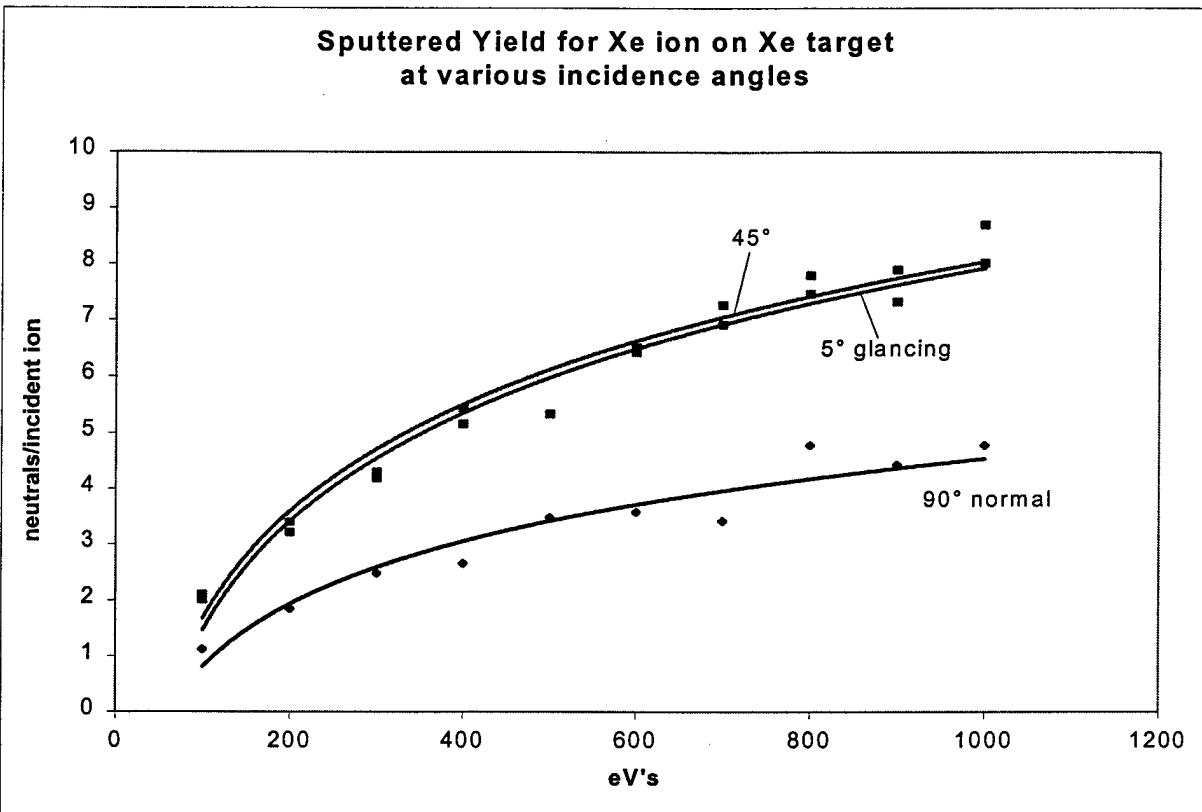
Figure 14: TRIM code sputtered yield for Xe+ ion impacting Xe condensate for various impact angles.
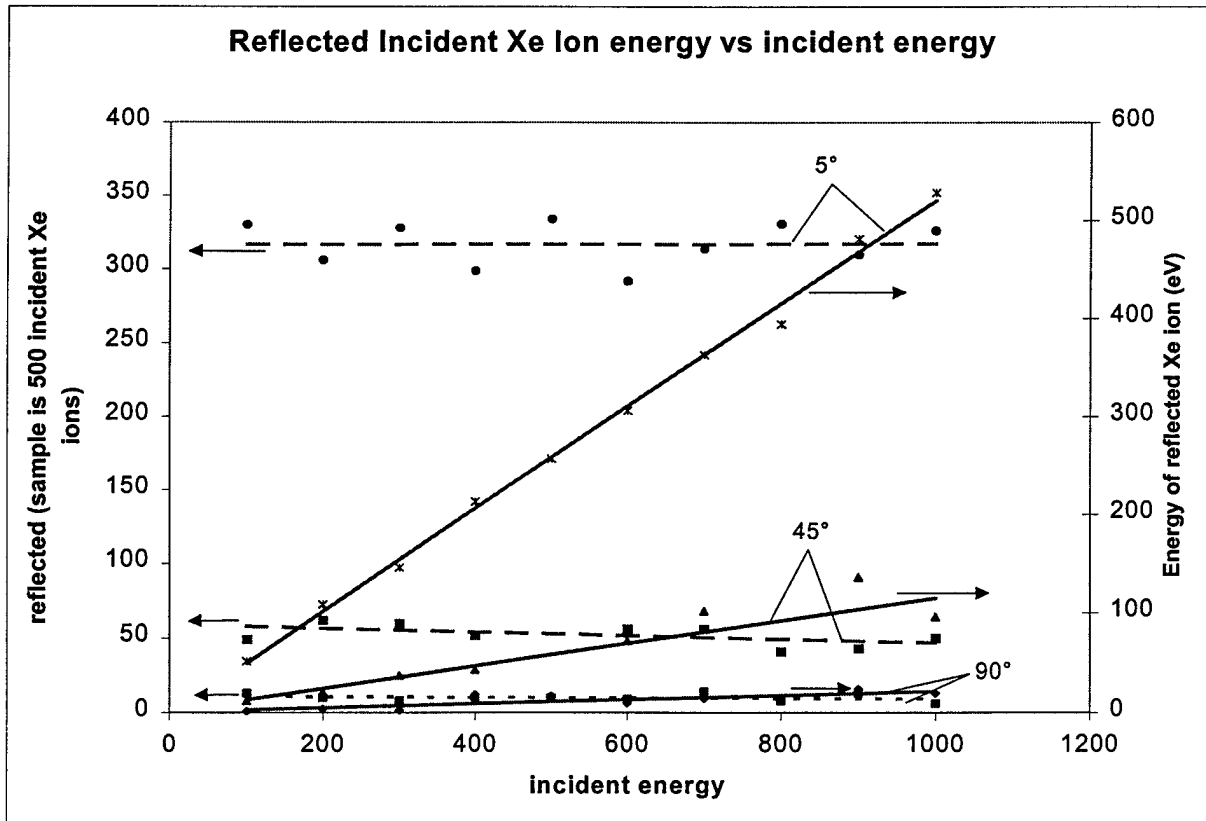
Figure 15: TRIM code - reflected Xe+ ions with associated energies vs Xe+ ion impact energy.
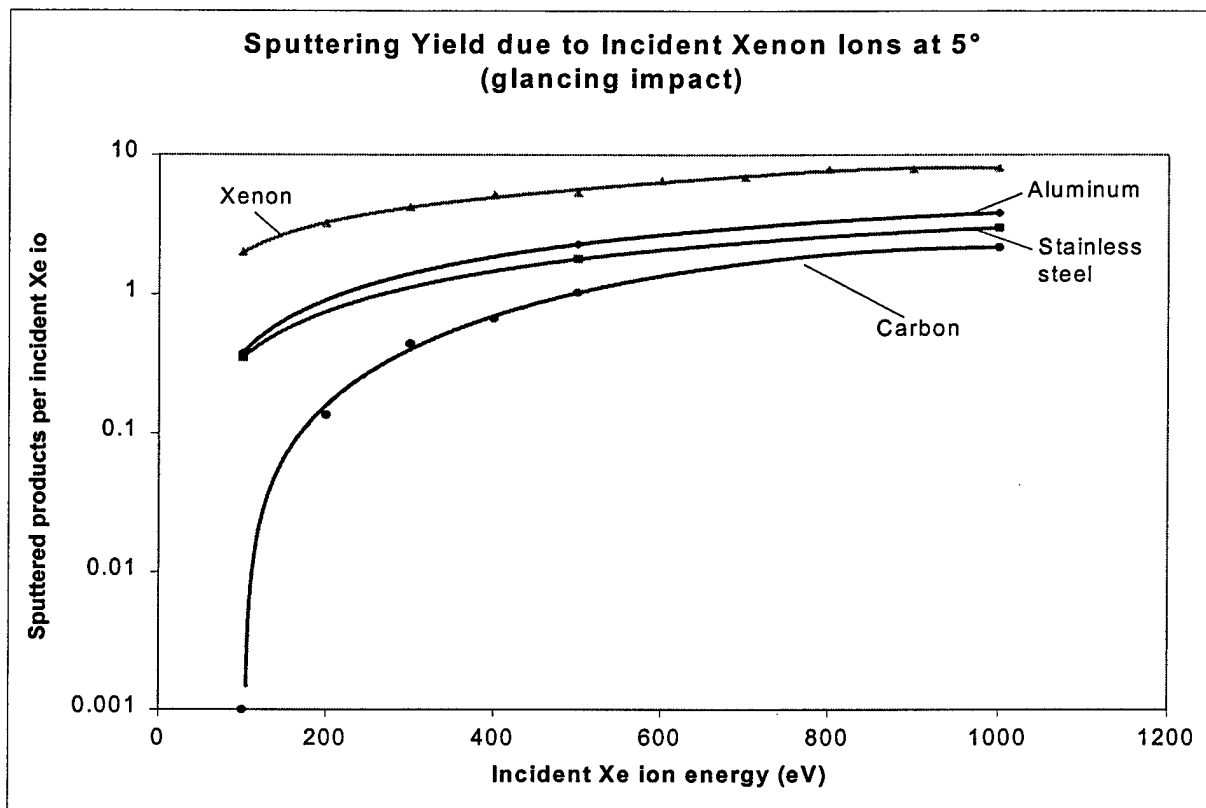
Figure 16: TRIM code - sputtered yield of various target material for glancing Xe+ ion impacts.
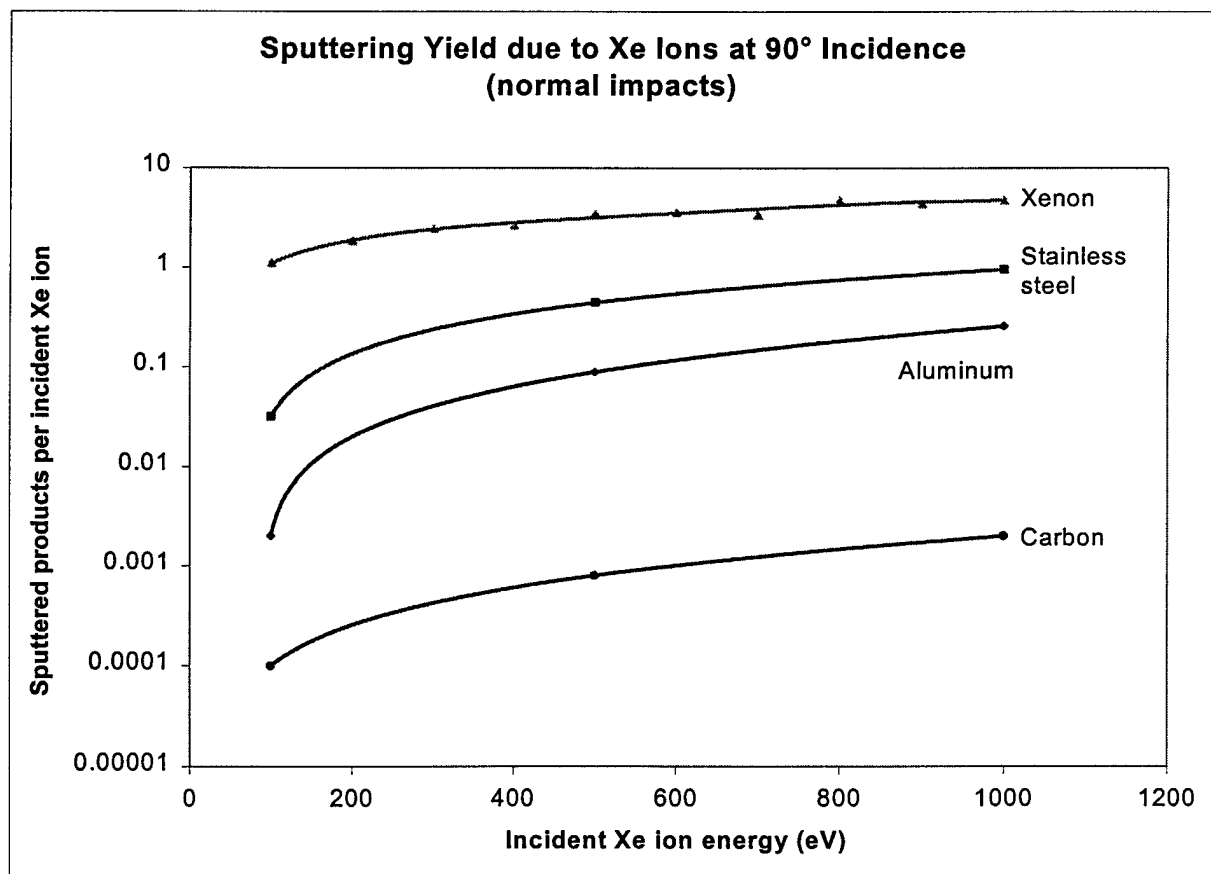
Figure 17: TRIM code - sputtered yield of various target material for normal Xe+ ion impacts.
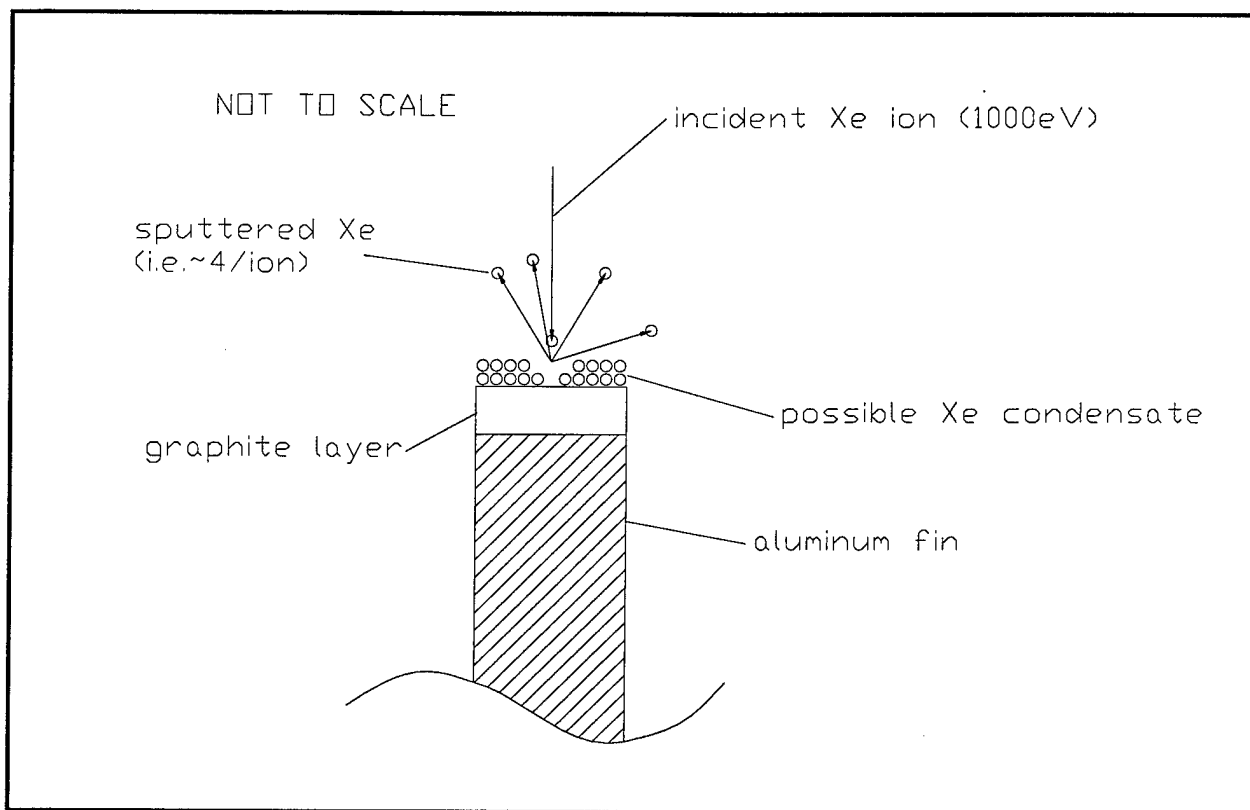
Figure 18: Rendition of the front edges of the aluminum cryo fins under Xe+ ion bombardment.
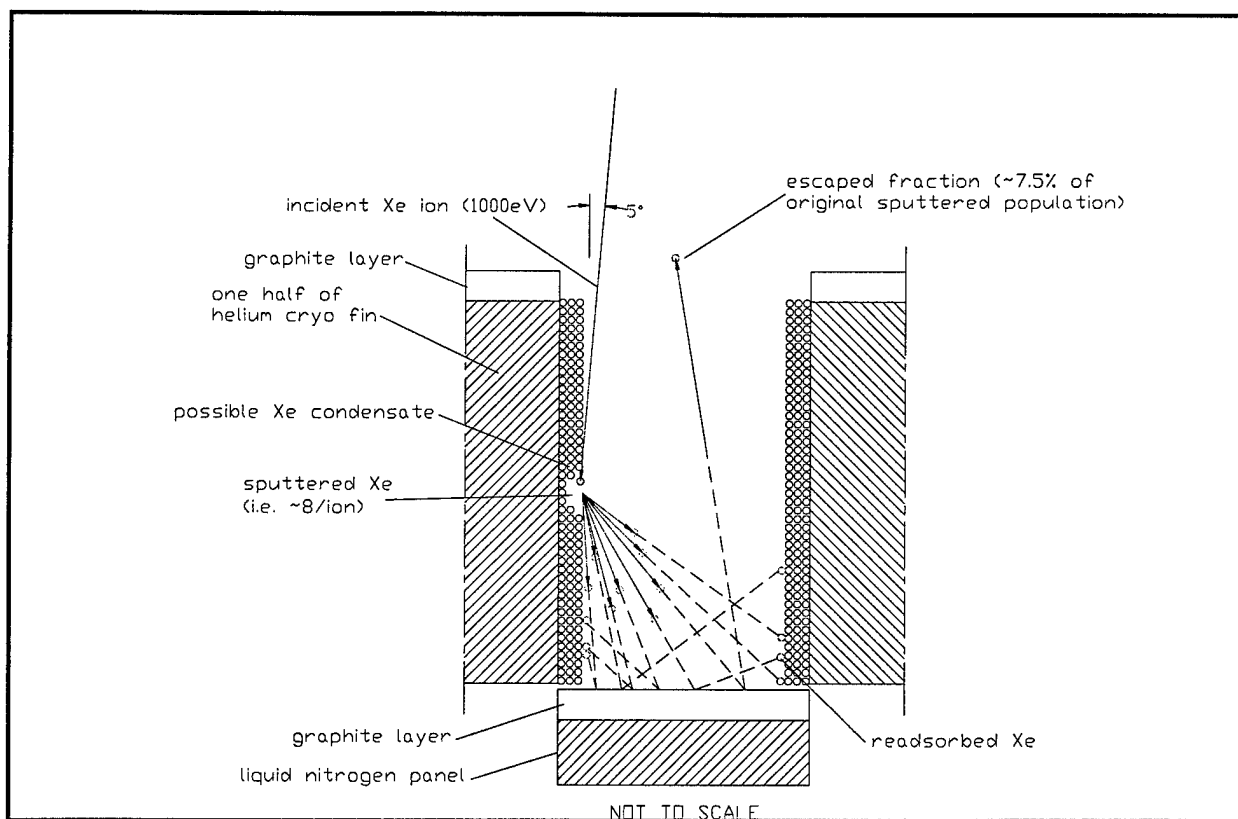
Figure 19: Rendition of the sides of the aluminum cryo fins under Xe+ ion bombardment.
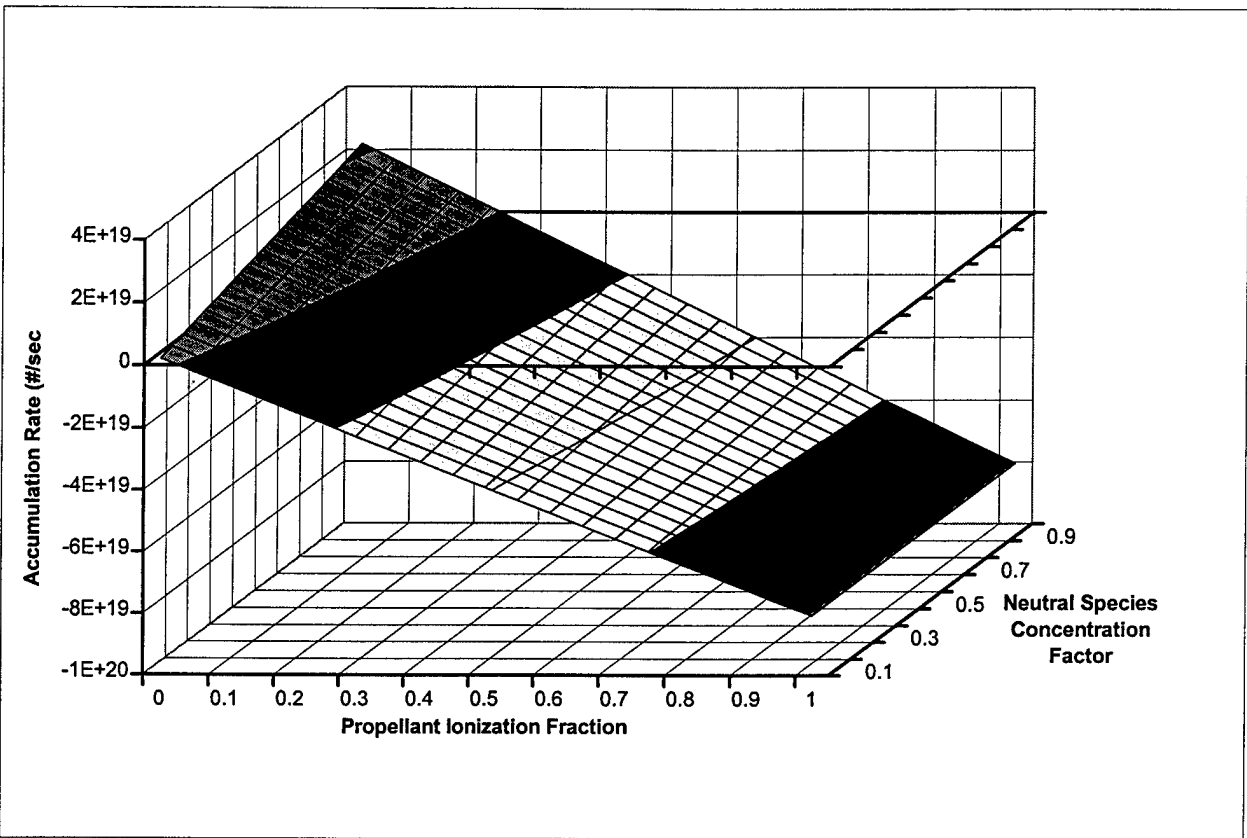
Figure 20: Accumulation rate of xenon condensate for normal impact angles (90°) [Eq. 14] (1 keV Xe+).
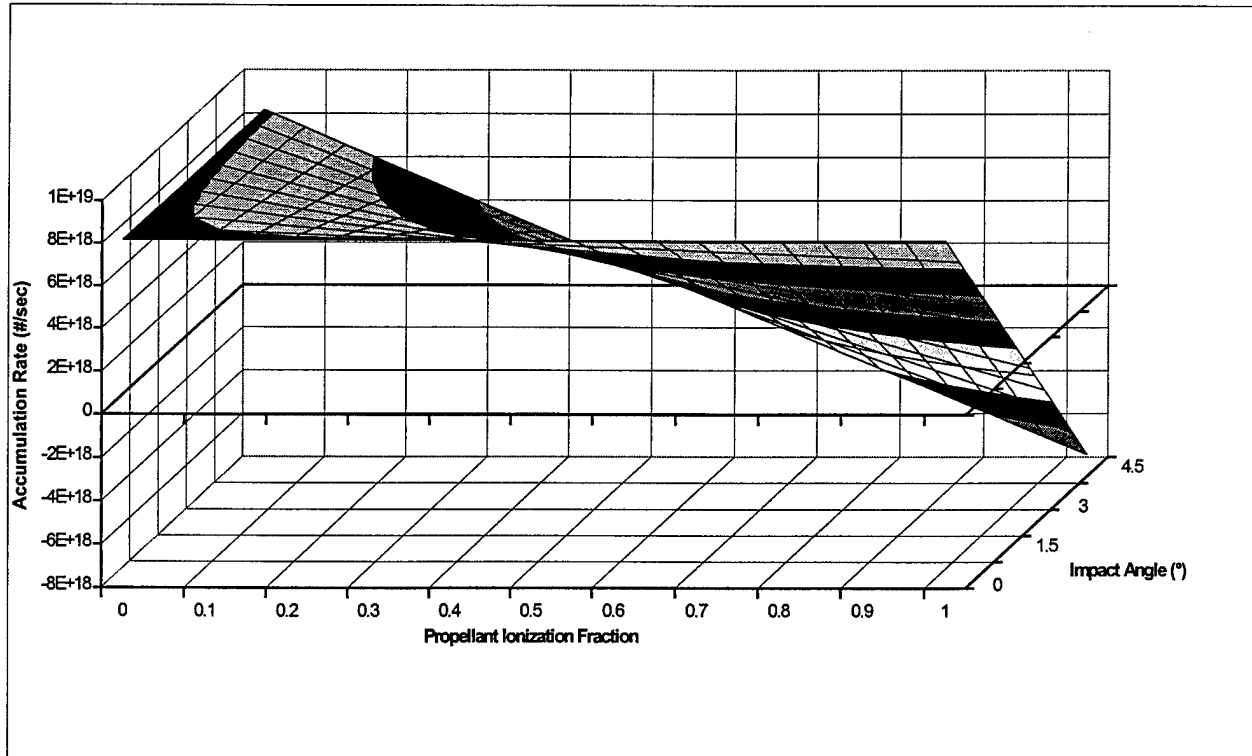
Figure 21: Accumulation rate of xenon condensate for side impact angles (5°) [Eq. 15] (1 keV Xe⁺).
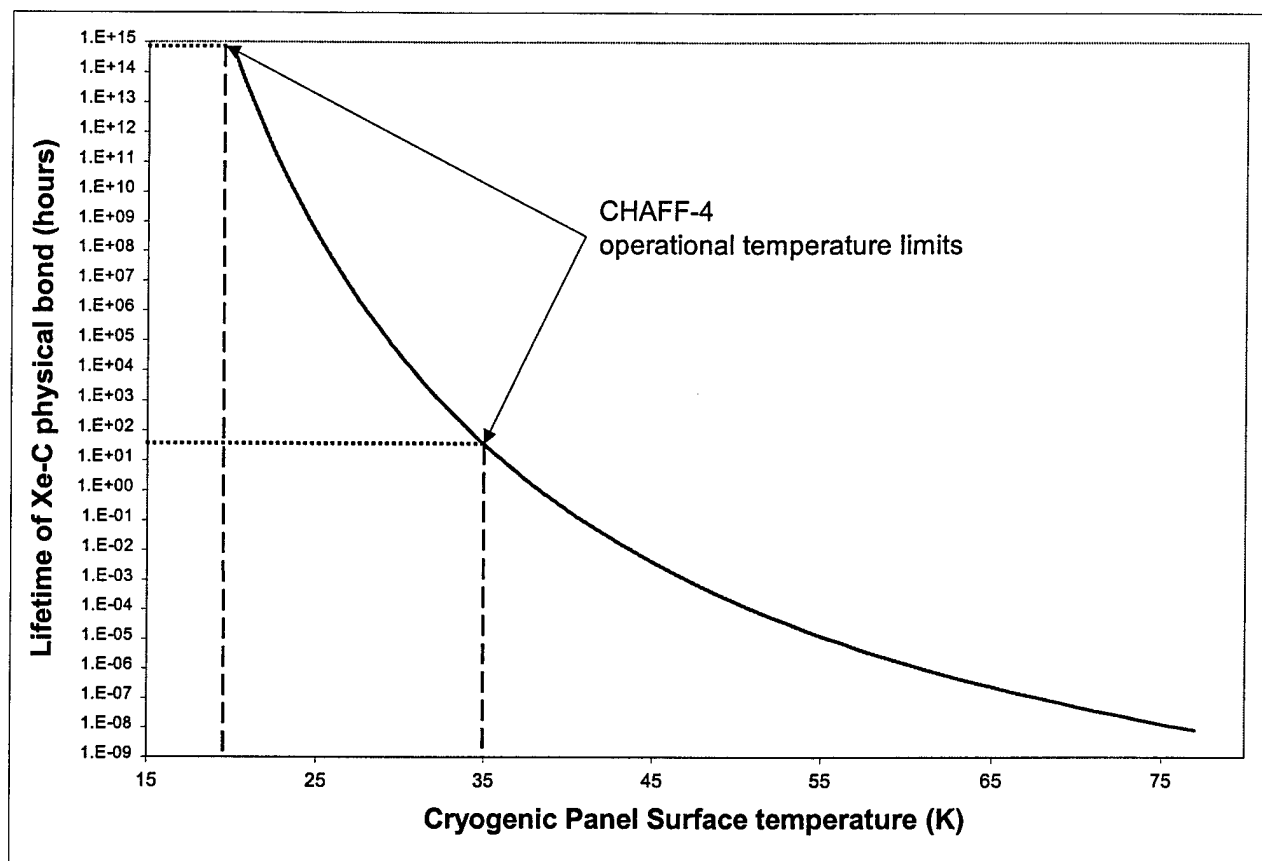
Figure 22: Estimated lifetime of Xe-C physical bond vs cryogenic shield array temperature.
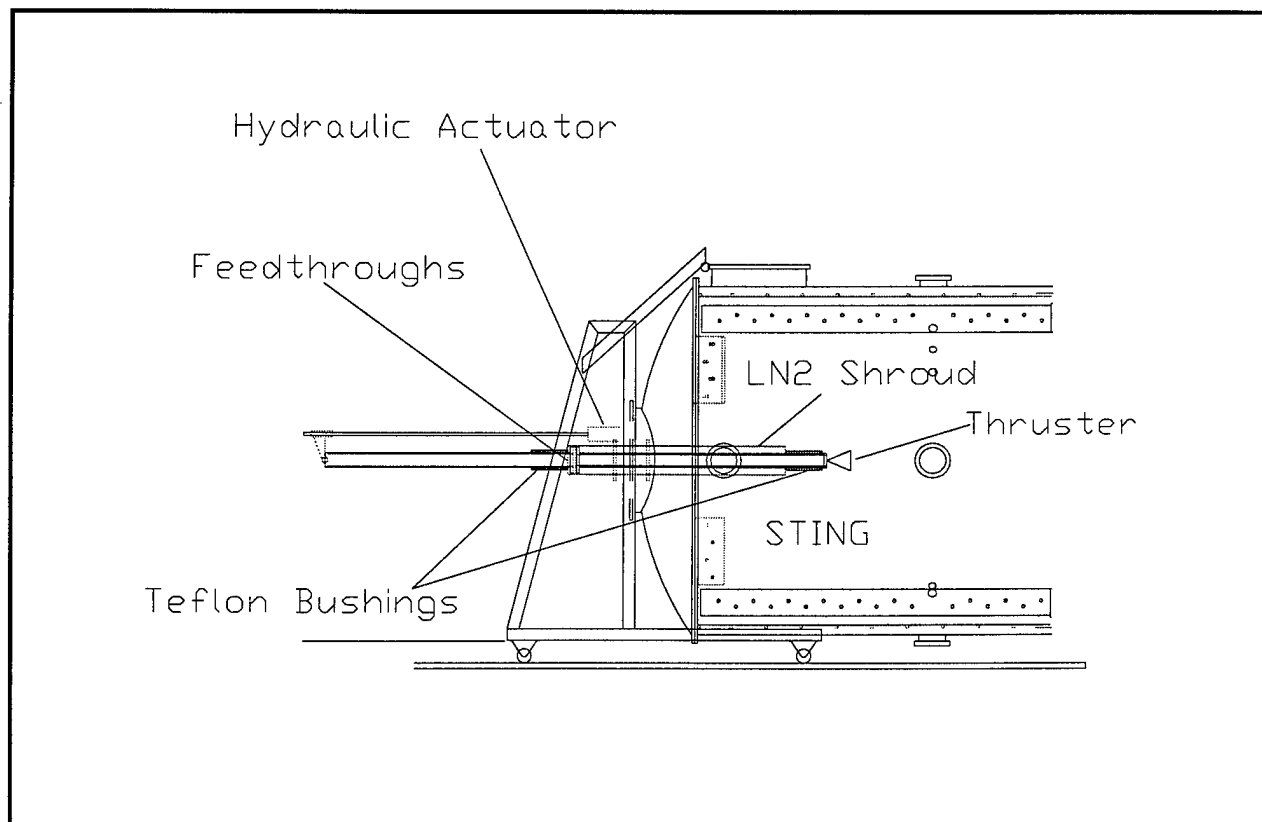
Figure 23: CHAFF-4's STING apparatus.
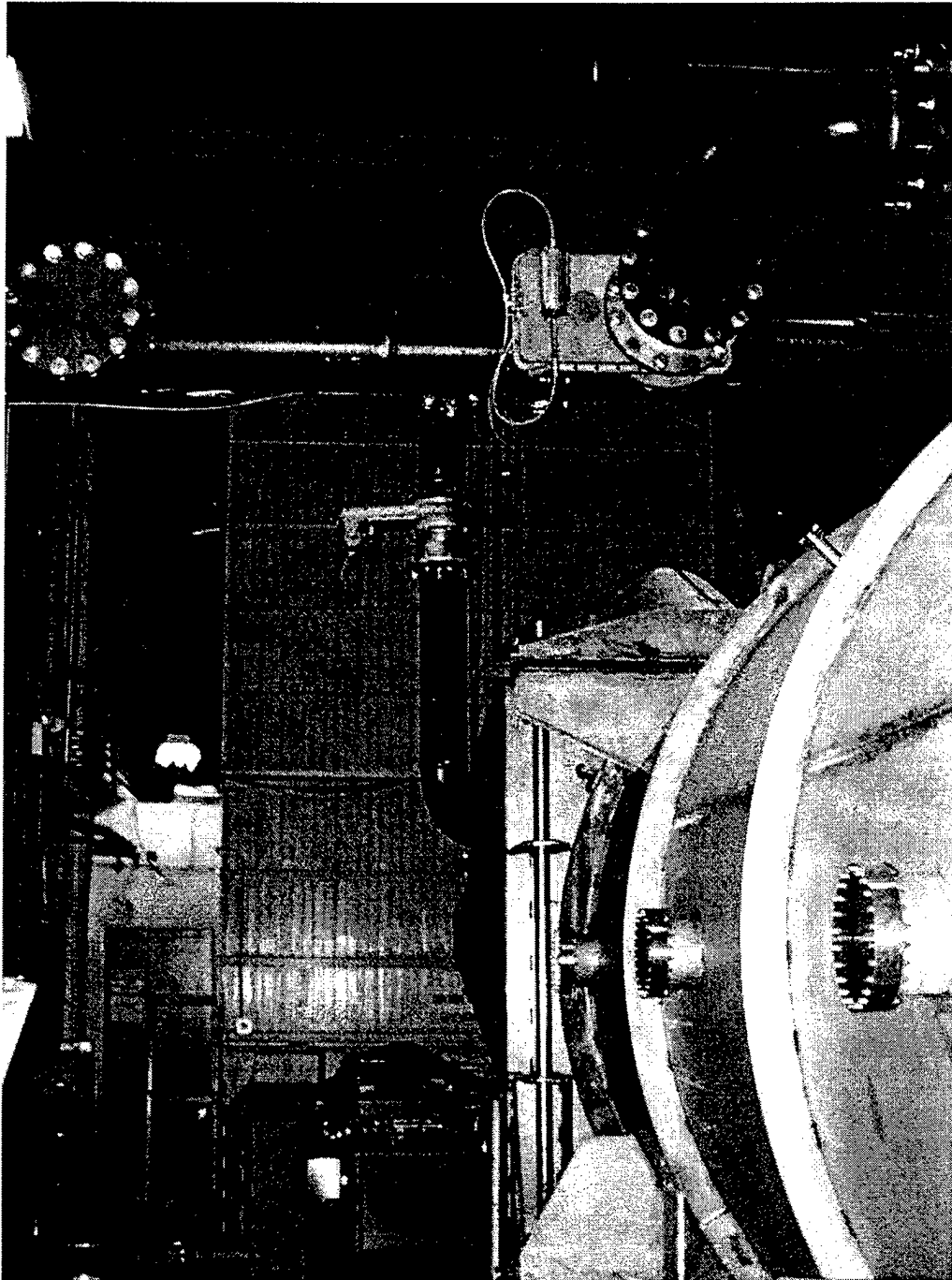
Figure 24: Side view of CHAFF-4. Note pump-down line from the roots blower system at top of picture.
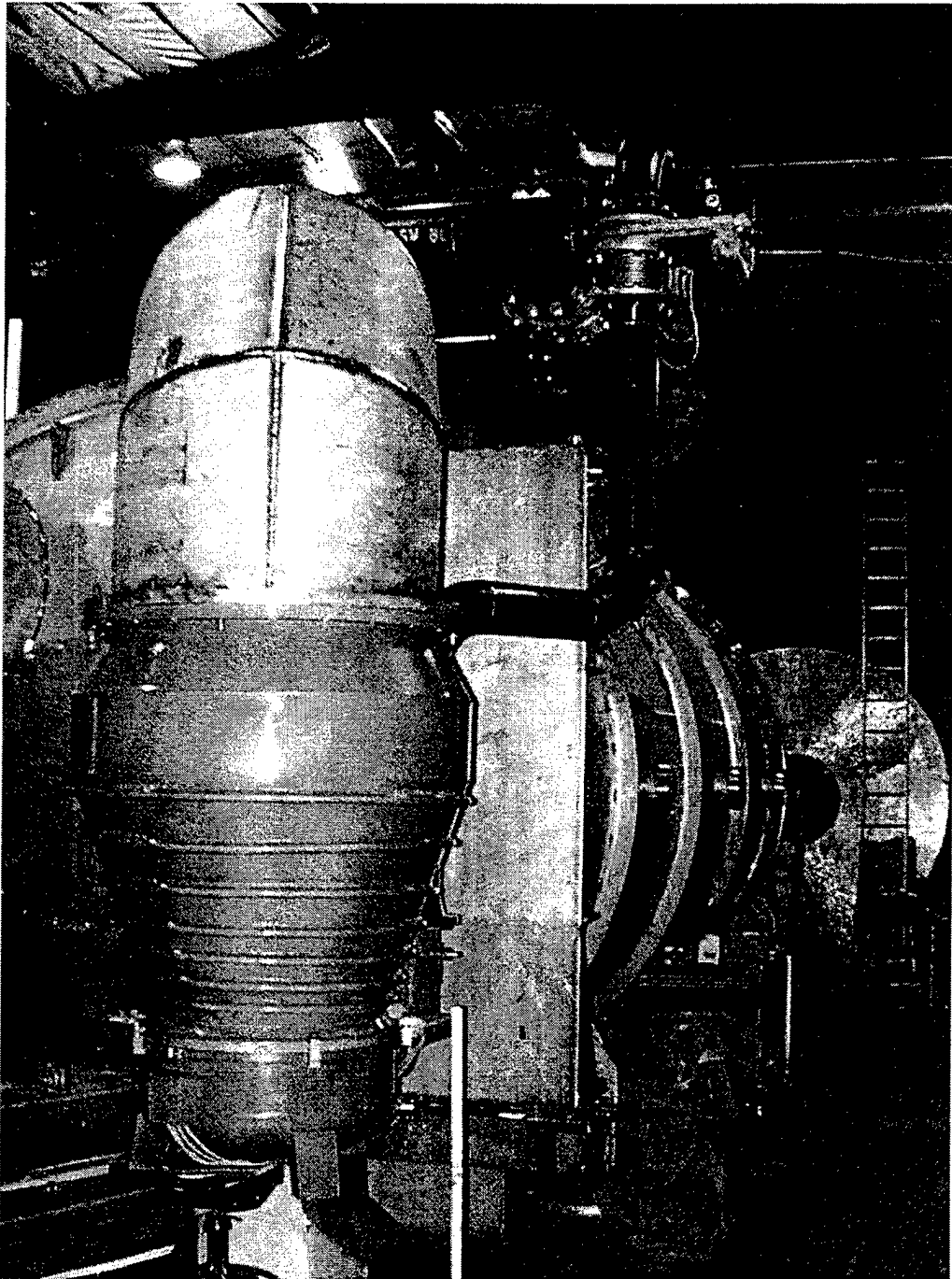
Figure 25:   Side view of CHAFF-4 highlighting one of two Zyrianka 900 diffusion pumps.
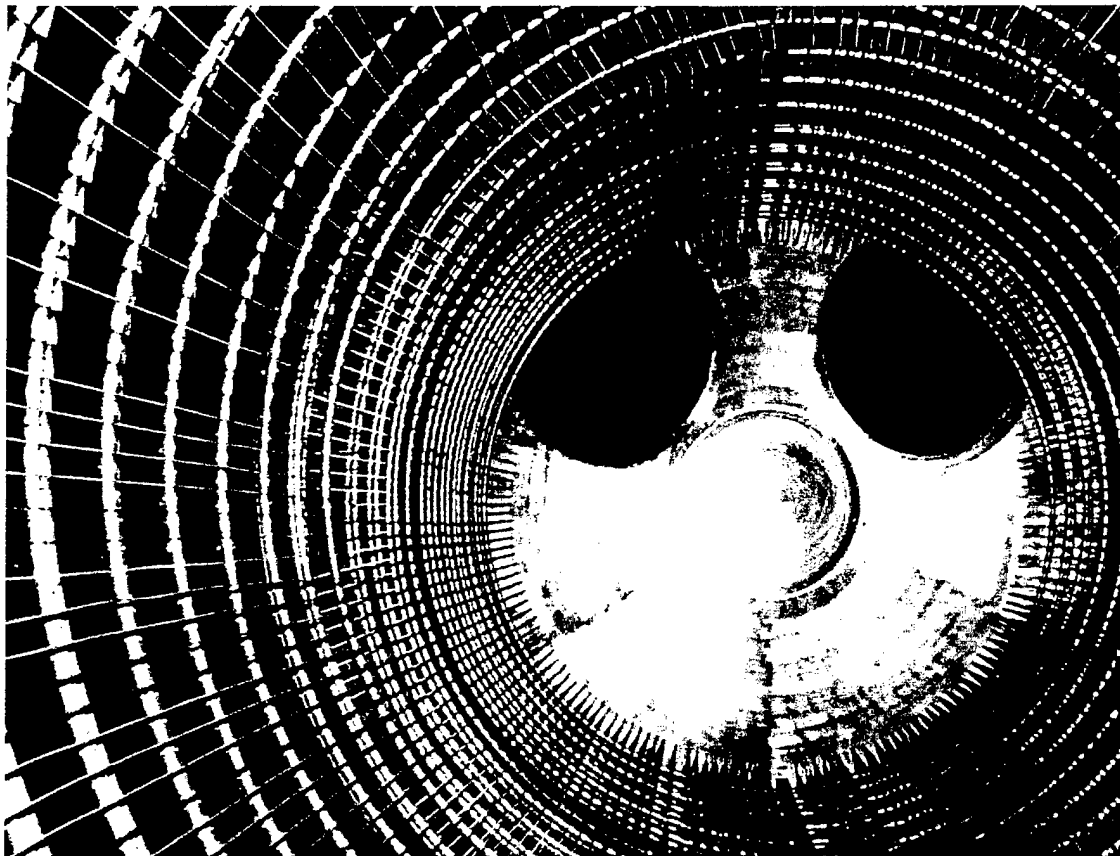
Figure 26: Part of the CHAFF-4 interior cryogenic shield system which will be maintained at 20 K.
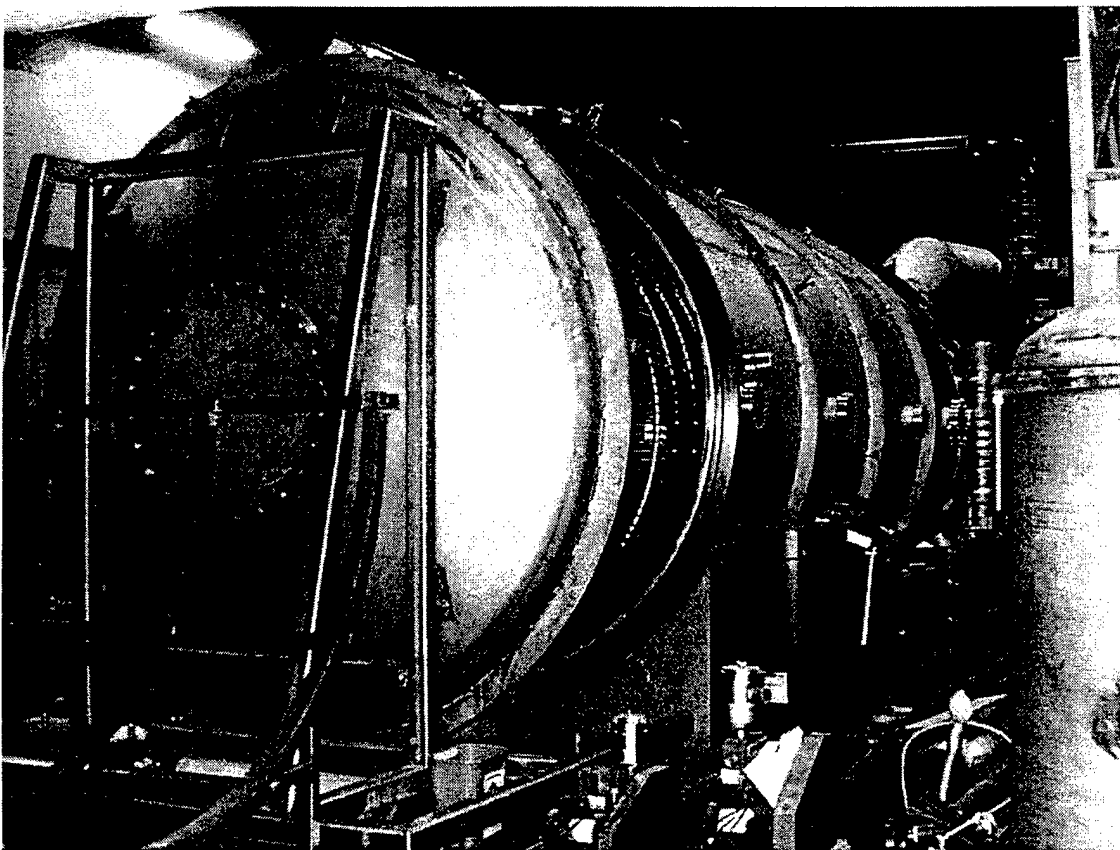

Figure 27: Side view of CHAFF-4 with sting side door partially open showing portion of inner shield.